

Slutrapport SBUF-projekt

Självverkande kylbaffelsystem

Slutrapporten följer i väsentliga delar dispositionen och texten i ansökan, men självverkande har ersatts med självreglerande.

ID: 12813

Jan-Olof Dalenbäck

Peter Filipsson

Jonas Gräslund

Anders Trüschel

Göteborg 2016-12-26

Innehåll

Bakgrund

Syfte

Genomförande

Tidplan

Organisation

Resultat

Redovisning

Bilagor

Filipsson, P., A. Trüschel, J. Gräslund and J-O. Dalenbäck (2016). **Induction ratio of active chilled beams – Measurement methods and influencing parameters.** *Energy and Buildings* 129, pp. 445–451.

Filipsson, P., A. Trüschel, J. Gräslund and J-O. Dalenbäck (2017). **A thermal model of an active chilled beam.** Submitted for publication in *Energy and Buildings*.

Bakgrund

Det finns olika vägar att uppnå hög energieffektivitet (minst samma nytta med mindre resurser) i nyproduktion eller vid renovering av kontorsbyggnader. En trend hos komponenttillverkare, installationskonsulter och högskolor är att utveckla tekniker för att aktivt behovsstyra via på kontorsplanen lokalt utplacerad styrutrustning såsom givare, spjäll och motorventiler i ventilationskanaler, rörsystem, tilluftsdon, radiatorer och kylbafflar som integreras i bus-system med belysning, passersystem, etc., för klimatisering.

En annan trend är att använda utrustning med få rörliga delar där behovsanpassningen av klimatet sker passivt. De ingående systemen är luftbehandlingsaggregat med batterivärmeväxling och låga lufthastigheter, frikyla till kylbaffelsystem som samtidigt ger värmeåtervinning till tilluften, samt självreglerande kylbaffelsystem. Dessa mer robusta och flexibla tekniklösningar vinner sakta mark via olika aktörer i de tre storstadsregionerna. Flera kontorsbyggnader utformade enligt ovan har varit i drift i flera år och fler är under uppförande.

System med självreglerande kylbafflar har, trots dyrare kylbafflar, lägre investeringskostnader än traditionella system tack vare att man kan använda oisolerade rörstråk och inte behöver någon styrutrustning i rummen. Det har i flera av de realiserade byggnaderna också visat sig att man har mindre än förväntade variationer med avseende på termisk komfort, även vid stora lastvariationer, med självreglerande kylbafflar. Det verkar finnas en eller flera faktorer som reducerar det installerade kyleffektbehovet och därmed även kylenergibehovet vid användning av kontinuerligt flöde av köldbärare vid rumstemperatur (inga styrventiler) jämfört med lägre temperatur på köldbärare och intermittert flöde (styrventiler). Kan man bestämma dessa faktorer kan man reducera installerad effekt och därmed reducera installationernas storlek i framtida projekt.

System med självreglerande kylbafflar ställer andra krav vid dimensionering än traditionella system. Men det saknas objektiva (mer vetenskapliga) utvärderingar med avseende på systemens utformning och funktion i de tillämpningar som beskrivs ovan.

Bättre empiriska (mätbara) och teoretiska kunskaper kring funktionen hos självreglerande kylbaffelsystem förväntas därför resultera i ökad kunskap om och användning av systemen. Vilket i sin tur förväntas ge ökade förutsättningar att förenkla drift och förbättra energieffektiviteten såväl i nybyggnation som vid renovering.

Ansökan avsåg ett doktorandprojekt i anslutning till Jonas Gräslunds verksamhet som adjungerad professor hos avdelningen för installationsteknik på Chalmers tekniska högskola.

Syfte

Syftet var att öka kunskapen om möjligheter och begränsningar med självreglerande kylbaffelsystem. Doktorandarbetet syftade dels till att beskriva funktionen hos system med självreglerande kylbafflar med kontinuerligt flöde av köldbärare vid rumstemperatur, såväl med

avseende på dess kapacitet att kyla i typiska kontorsrum (energi/effekt) som med avseende på termisk komfort i kontorsrummen, samt till att jämföra funktionen hos självreglerande kylbafflar med motsvarande funktion hos traditionell teknik med intermittert styrt flöde av köldbärare med lägre temperatur än rumstemperaturen.

Genomförande

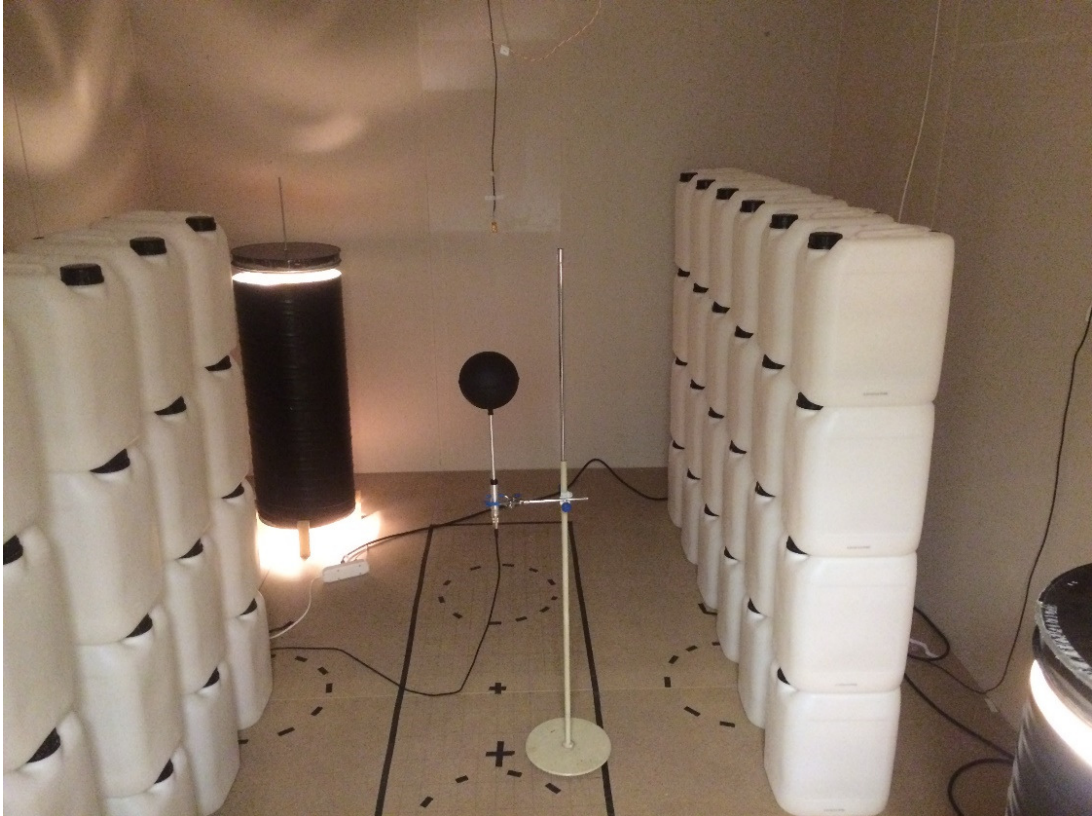
Projektet genomfördes som ett forskningsprojekt av en doktorand, Peter Filipsson, hos avdelningen för Installationsteknik, vid Chalmers tekniska högskola. Projektet kom att genomföras i anslutning till ett pågående forskningsprojekt där en annan doktorand (M. Gruber) verifierat funktionen hos framkopplad styrning av termiskt komfort och luftkvalitet i ett kontorsrum i avdelningens försökshall. Det gav stora möjligheter till kunskapsöverföring samtidigt som kostnaderna för de laborativa undersökningarna kunde begränsas.



Kylbaffel installerad i Installationstekniks försökshall (labb).

Doktorandarbetet byggde inledningsvis på litteraturstudier och obligatoriska doktorandkurser. De planerade fältstudierna i redan utförda byggnader med såväl traditionellt utformade kylbaffelsystem (t.ex. Hagaporten 3, Solna) som med system med självreglerande kylbafflar (t.ex. Gångaren 16, Stockholm), genomfördes på en övergripande nivå. Arbetet inriktas istället främst på att studera system med självreglerande kylbafflar mer i detalj i Installationstekniks labb. Fältstudiespåret har dock åter tagits upp i slutet av projektet och kommer sannolikt att resultera i en vetenskaplig artikel.

Arbetet kom då att omfatta teoretiska beräkningar (Matlab, mm) av den värmetekniska funktionen hos självverkande och traditionella kylbaffelsystem och verifiering av desamma genom mätningar under väl kontrollerade förhållanden i laboratoriemiljö. Först studerades hur luft- och vattenflöden med olika temperaturer inverkade på medejekteringen av rums-luft (induction ratio = IR). Dessa mätningar låg sedan till grund för att utveckla och verifiera en modell av en kylbaffell. I slutskedet av projektet studerades också inverkan av värmetrögheten hos byggnadsstomme och rumsinredning.



Försöksrummet i Installationstekniks labb. Uppe till vänster och nere till höger i bild syns utrustning för internvärmegenerering. I mitten syns givare för mätning av globtemperatur och vattendunkarna användes för att variera rummets termiska tröghet.

Den högre temperaturnivån på köldbäraren i det självreglerande systemet möjliggör större andel frikyla och därmed mindre andel köpt energi. Då kan också frikyla med värmeväxlare i luftbehandlingsaggregatet komma att studeras. Planerade studier av sambanden mellan kyllösningen och kylenergianvändningen kommer att studeras och kvantifieras i en andra fas (Se ansökan).

Tidplan

Ansökan omfattade en första fas, med projektstart 1 april – 1 juli, 2013, som förväntades leda fram till en licentiatavhandling och projektslut 1 oktober - 31 dec 2015. De olika planerade delarna i forskningsprojektet redovisas i nedanstående tidplan. En andra fas under 2016-2018 förväntades sedan leda fram till en doktorsavhandling.

	2013	2014	2014	2015	2015
Litteraturstudier					
Doktorandkurser					
Fältmätningar					
Modeller					
Beräkningar					
Verifiering i labb					
Artiklar					
Lic-avhandling					

Planerad tidplan

	2014	2015	2015	2016	2016
Litteraturstudier					
Doktorandkurser					
Fältmätningar					
Modeller					
Beräkningar					
Verifiering i labb					
Artiklar					

Verklig tidplan

Då doktorandprojektet genomförts av en industridoktorand istället för en anställd doktorand har projekttiden fördröjts ett år på grund av en senare projektstart. Ovanstående tidplan visar hur projektet genomförts. Den andra fasen som ska leda fram till en doktorsavhandling förväntas därför påbörjas under 2017 och sträcka sig fram till 2019.

Organisation

Projektet har letts av Jonas Gräslund, SKANSKA (adjungerad professor och biträdande handledare) och forskningsprojektet har genomförts av en industridoktorand, Peter Filipsson, inskriven hos avdelningen för Installationsteknik, Chalmers tekniska högskola.

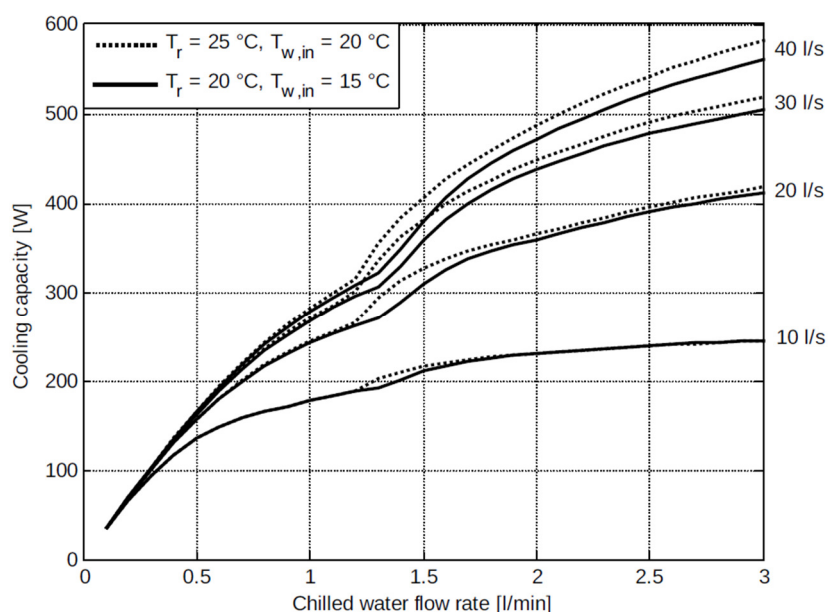
Utöver ovanstående har **projektgruppen** bestått av Jan-Olof Dalenbäck (professor, examinator och huvudhandledare) och universitetslektor Anders Trüschel (universitetslektor och biträdande handledare).

Projektets **referensgrupp** har omfattat Ivo Martinac (professor, installationsteknik, KTH), Dennis Johansson (avdelningschef, installationsteknik, LTH), Anders Bernestål (Andersson & Hultmark), Roger Linman (NCC), Maria Sörensson (Ventab), Jörgen Persson (ÅF) och Thomas

Eastwood (Bravida). Referensgruppen har haft tre möten med varierande deltagande under projekttiden.

Resultat

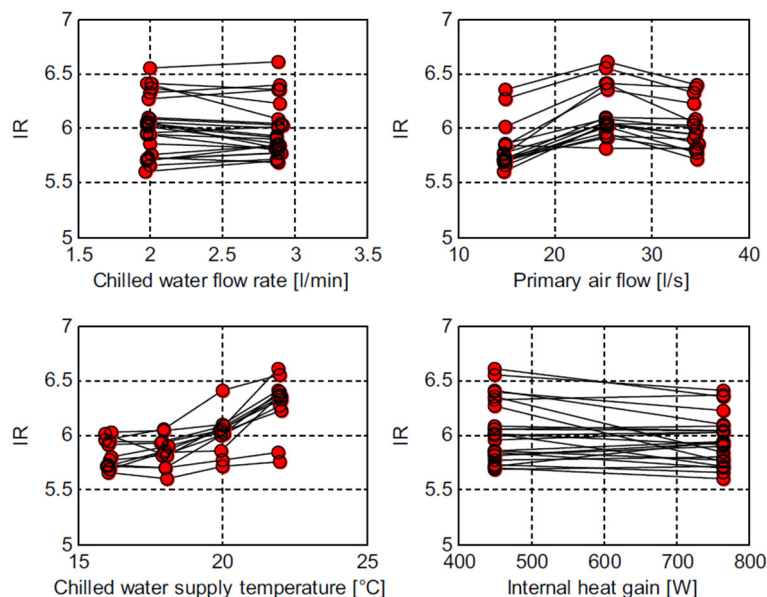
Det främsta resultatet av projektet är **en ny teoretisk modell av en kylbaffel** som kommer att implementeras i IDA ICE. Modellen redovisas i detalj i bifogad vetenskapliga artikel **”A Thermal Model of an Active Chilled Beam”** som sänts in för publikation i *Energy and Buildings* (Elsevier). Modellen bygger på NTU-metoden och har verifierats genom mätningarna i labbet. Nedanstående diagram visar beräkningar med modellen för den testade kylbaffeln.



Kylbaffelns kyleffekt som funktion av köldbärarflöde och tilluftsflöde vid två olika kombinationer av köldbärartillopps- och rumstemperatur.

Modellens fördelar jämfört med befintliga modeller är dess höga noggrannhet, att den beräknar köldbärarflöde vid delast (vilket krävs för att bestämma köldbärarpumparbete), samt att den beräknar flöde och temperatur på luften som lämnar kylbaffeln. Det sistnämnda är väldigt passande nu när allt fler byggnadssimuleringsprogram utvecklas från att räkna med homogen lufttemperatur i hela rummet till att bli CFD-modeller med information om luftrörelser och hur temperaturen varierar i alla punkter i rummet. Ovan nämnda fördelar är inte begränsade till självreglerande kylbafflar utan gäller även traditionellt styrda kylbafflar.

Dessförinnan genomfördes mätningar där medejkteringen av rumsluft bestämdes på olika sätt. Dessa resultat har publicerats i bifogad vetenskaplig artikel **”Induction Ratio of Active Chilled Beams - Measurement 1 Methods and Influencing Parameters”** i *Energy and Buildings* (Elsevier).



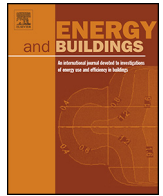
Kylbaffelns medejkeringskvot (IR) som funktion av köldbärarflöde, tilluftsflöde, köldbärartemperatur och internvärmelast.

Förutom att presentera nya sätt att mäta en kylbaffels medejkeringskvot (IR) så visades även att denna beror på köldbärartemperaturen, vilket är till högtempererade kylbafflars fördel (se diagram ovan).

Redovisning

Forskningsresultaten har redovisats i två vetenskapliga artiklar i ***Energy and Buildings*** (Elsevier), se bilagor, och kommer att redovisas i en populärvetenskaplig artikel i ***Energi&Miljö***. Dessutom har delresultat av projektet redovisats vid ett teknikseminarium om kyla anordnat av Energi- och miljötekniska föreningen i februari 2015 och senare vid konferensen ***IBPSA BuildSim-Nordic*** i Trondheim i september 2016. Presentationen kan laddas ner från <http://ibpsa-nordic.org>.

Projektet kommer dessutom att presenteras vid ett seminarium för branschens aktörer där SBUF involveras att bjuda in sina medlemsföretag. Då projektet redovisats i vetenskapliga artiklar av en industridoktorand kommer det inte att publiceras i planerad licentiatuppsats, som endast skulle omfatta en sammanfattning av resultaten tillsammans med de två vetenskapliga artiklarna.



Induction ratio of active chilled beams – Measurement methods and influencing parameters



Peter Filipsson^{a,b,*}, Anders Trüschel^a, Jonas Gräslund^{a,c}, Jan-Olof Dalenbäck^a

^a Division of Building Services Engineering, Department of Civil and Environmental Engineering, Chalmers University of Technology, 412 96, Gothenburg, Sweden

^b CIT Energy Management AB, 412 88, Gothenburg, Sweden

^c Skanska Commercial Development Nordic AB, 112 74, Stockholm, Sweden

ARTICLE INFO

Article history:

Received 11 May 2016

Received in revised form 25 July 2016

Accepted 5 August 2016

Available online 6 August 2016

Keywords:

Active chilled beams

Induction ratio

Entrainment ratio

Measurements

ABSTRACT

In active chilled beams, primary air from the air handling unit induces room air which passes a cooling coil before it mixes with the primary air and discharges into the room. The ratio of induced room air flow to the primary air flow is the induction ratio (IR). Knowledge about the IR is important when modelling cooling capacity as well as temperature and velocity of the air discharged from the beam.

Most previous studies of the behavior of IR are focusing on the influence of primary air flow. The purpose of the work presented in this paper is to investigate whether other operating conditions also influence the IR. Three methods of determining the IR are compared in order to strengthen the conclusions.

The results indicate that the IR is influenced by the chilled water temperature due to buoyant forces. Novel methods of determining the IR are presented and it is concluded that current methods may lead to overestimation.

© 2016 Elsevier B.V. All rights reserved.

1. Introduction

Active chilled beams have gained increased recognition as a sustainable comfort cooling technology with favorable performance regarding energy efficiency, peak power demand, thermal comfort and economy.

1.1. Active chilled beams

Active chilled beams are provided primary air from the air handling unit and water from a chilled water system. The chilled water is circulated in a hydronic cooling coil inside the active chilled beam. The primary air enters the room via a pressure plenum and several nozzles along the beam. The high air velocity generated by the nozzles reduces the static pressure and induces room air that passes the coil before it mixes with the primary air. The mixed air is discharged into the room through slots along both long sides of the beam (see Fig. 1).

A key opportunity with active chilled beams is utilization of high temperature cooling. This provides major benefits such as increased use of free cooling, better performance of chillers, reduced risk of condensation (reduced latent load), reduced losses in the chilled water distribution system and less need for individual room control. For example, Gräslund [1] presents a high temperature active chilled beam system without chillers and room thermostats. The water is chilled in boreholes and by preheating incoming outdoor air (when needed) and due to the self-regulating characteristic of high temperature cooling there is no individual room control of chilled water flow rate.

However, in the absence of individual room controls, accurate simulation models are needed when dimensioning the cooling system. Typically, worst-case scenarios or crude safety margins are used when designing comfort cooling systems. The safety margins are compensated for by the room control and the only consequence is oversized equipment. In a system without individual room control on the other hand, any overestimation of the cooling load will impact the room air temperature.

1.2. Induction ratio

The ability of recirculating room air is often expressed as the induction ratio (other names such as entrainment ratio and mixing ratio are also common in the literature). In this paper, the induc-

* Corresponding author at: Division of Building Services Engineering, Department of Civil and Environmental Engineering, Chalmers University of Technology, 412 96, Gothenburg, Sweden.

E-mail addresses: filipssp@chalmers.se (P. Filipsson), anders.truschel@chalmers.se (A. Trüschel), jonas.graslund@skanska.se (J. Gräslund), jan-olof.dalenback@chalmers.se (J.-O. Dalenbäck).

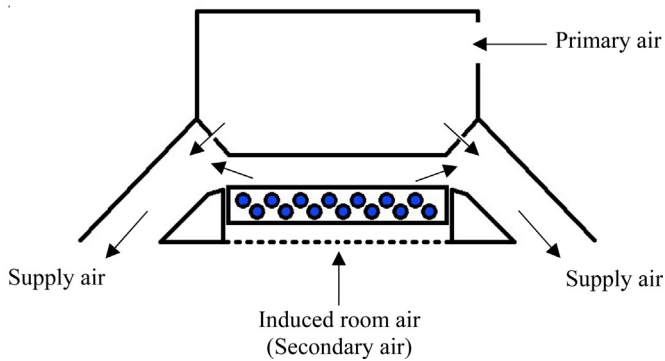


Fig. 1. Schematic diagram of a common type of active chilled beam.

tion ratio (IR) is defined as the ratio of the secondary air volume flow rate to the primary air volume flow rate (other definitions are also common in the literature). A high IR is crucial in order to achieve good heat transfer since a large flow of induced air increases both the airside convective heat transfer coefficient of the coil and the driving temperature difference. Knowledge about the induction ratio is necessary when making indoor climate simulations since it determines temperature and flow rate of supply air.

Furthermore, one of the most significant uncertainties in peak cooling load calculations is the convective heat transfer coefficient of the thermal mass in the building [2]. Correlations of convective heat transfer coefficient for forced convection are based on the supply air flow [3] and rooms equipped with active chilled beams are no exception [4]. Knowing the IR is thereby important in order to determine the peak cooling load.

1.3. Previous studies of induction ratio

In contrast to passive chilled beams, in which the convective heat transfer is natural, active chilled beams are characterized by forced convection. However, a buoyant force does act on the warm air moving upwards across the cold coil [5]. It is important to keep in mind that the buoyant force in a passive beam acts in the same direction as the air flow while it counteracts the air flow in most active chilled beam designs.

A cooler coil gives a higher buoyant force slowing down the upwards moving warm air. Regarding the temperature of the room air however its influence is harder to predict. On the one hand, warmer air will be slowed down more because of the larger temperature difference. But on the other hand, warmer air is lighter and more easily elevated by the inductive force.

Most existing studies on how the induction ratio is influenced by the operating conditions are focusing on primary air plenum pressure and primary air flow. Results from Ruponen and Tinker [6] and from Guan and Wen [7] shows a weak negative correlation between primary air plenum pressure and IR while Chen et al. [8] shows a weak positive correlation. Results from Hyun et al. [9] shows a peak in IR at a certain pressure and both increasing and decreasing the pressure give a slight decrease of IR. Rhee et al. [10] shows that the IR does not seem to be influenced by the primary air flow rate. Cammarata and Petrone [11] use CFD-modelling to determine the IR and concludes that it is very insensitive to variations in the primary air velocity.

Thus, a number of studies have been made in order to see how IR is related to primary air flow and the general conclusion is that the correlation is weak or nonexistent. Meanwhile, it is known that buoyant forces act on the non-isothermal air moving in a vertical direction across the coil. Freitag et al. [12] investigate how the IR is influenced by the temperature difference between chilled water and room air. It is concluded that a larger difference gives a lower IR

but the influence is not considered strong enough to call for changes in the design of active chilled beams with respect to this finding.

IR is often expressed as a function of primary air flow and/or plenum pressure when modelling active chilled beams [8,13,14]. Livchak et al. [5] adds a term proportional to the temperature difference between the induced air and the chilled water when calculating the induced air flow in order to capture the influence of buoyant forces.

Furthermore, there are studies made on how IR is influenced by the design of the supply air outlet, nozzles and geometry of the plenum, based both on measurements [15,19] and on CFD-analysis [16].

1.4. Determination of induction ratio

The primary air flow is relatively easy to determine by measuring the pressure drop over an orifice plate with known air flow rate constant in the primary air duct. But in order to calculate the IR it is necessary to determine the flow of induced air which is more difficult. Following is a summary of known methods.

1.4.1. Capacity

A common method is applying an energy balance over the chilled coil. By measuring the flow and the temperature rise of the chilled water and the temperature drop of the induced air the flow of induced air can be determined. A major drawback of the method is the issue of measuring the temperature of the induced air downstream the coil [8]. Ruponen and Tinker [6] concluded that this method overestimated the IR by at least 25%. They pointed out that the error may come from the non-flat velocity profile of the induced air passing the coil. Their temperature sensor was placed in the middle of the coil where the velocity probably exceeded the average. Additional problem with measuring the induced air temperature downstream the coil is the non-uniform temperature of the coil. The temperature varies both along and across the coil which makes it very hard to find a representative temperature. On top of that, the induced air is mixed with the primary air very soon after leaving the coil. Another problem is that heat radiated to the coil increases the water temperature without decreasing the air temperature which cause an overestimation of the air flow.

1.4.2. Temperature

Rhee et al. [10] used a method of measuring the temperature of the mixed supply air, the primary air and the induced air downstream the coil to calculate the IR. Just as the capacity method, this method suffers from the problem of measuring the induced air temperature downstream the coil.

1.4.3. Air velocity

Ruponen and Tinker [6] presented a single purpose built measurement venturi with which it is possible to determine the induced air flow rate as a function of the air velocity measured in one point in the throat of the venturi. It was concluded that the method produces reliable and consistent results.

Chen et al. [17] used a velocity transducer to scan the induced air velocity in a dense grid under the beam. The purpose in this study was to determine the velocity profile but the method can be used to determine air flow rate as well.

Guan and Wen [7] installed an external hood at the supply air outlets. The hood was long enough to reduce the turbulence of the supply air and the velocity at the end of the hood was measured with a velocity transducer at 19 points along each long side of the beam.

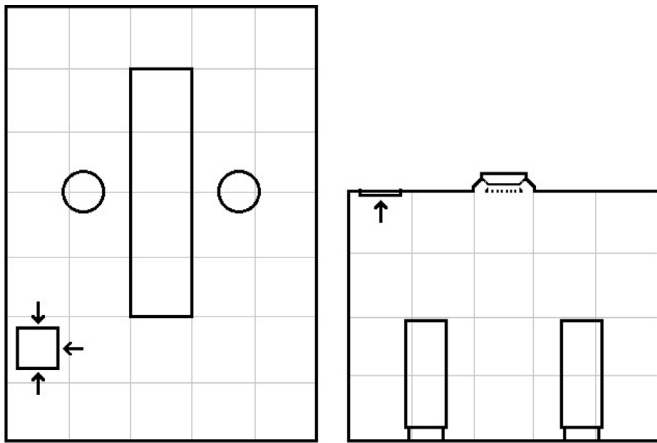


Fig. 2. Layout of the room and positions of active chilled beam, exhaust air terminal device and dummies. Top view to the left and front view to the right. Grey lines indicate a distance of 0.6 m.

1.4.4. Pressurized chamber

The British Standard BS 4954-1 [18] describes a method for measurement of IR of induction units in general. Two pressurized chambers are used to determine the flow of supply air. The chamber pressure is controlled by regulating the air flow out of the chamber. Ruponen [19] reports that this method is more suitable for other types of induction units with lower IR than it is for active chilled beams with relatively high IR.

1.5. Objective

The objective of this work is to study how the IR is influenced by several operating conditions including temperatures of chilled water and room air. The study includes three methods to determine the IR, one based on air velocity, one based on an energy balance and one based on concentrations of a tracer gas.

2. Methodology

The work presented in this study is divided into two parts. The first part is a comparison of three fundamentally different methods of measuring IR. In the second part, one of the methods is used to investigate whether IR is influenced by the operating conditions (temperature and flow rate of chilled water, flow rate of primary air and level of internal heat gain). All experiments are made with a 2.4 m × 0.6 m Halton CBS active chilled beam.

2.1. The test room

The measurements were carried out in a full-scale mockup of an office room (see Fig. 2). The internal dimensions of the room were 3.0 m × 4.2 m × 2.4 m (width × length × height). The active chilled beam was positioned in the suspended ceiling in the middle of the room and two thermal dummies (cooling load simulators) were positioned on each side of the active chilled beam at half of the distance between the center and the long side of the room. The temperature outside the room was controlled to not deviate more than 2 °C from the temperature inside the room in order to minimize heat transfer through the envelope of the room. The walls were made of 12 mm plasterboard attached on the inside of 100 mm expanded polystyrene. The floor was made of 22 mm fiberboard on top of 6 mm plasterboard and 30 mm expanded polystyrene.

Table 1
Description of the studied cases.

	Primary air flow rate q_p [l/s]	Supply chilled water temp. $t_{w,in}$ [°C]	Room air temp. t_r [°C]
1	25	20	25
2 ^a	25	20	25
3	25	16	25
4	25	14	25
5	35	20	25
6	15	20	25
7	25	20	21
8	25	20	31

^a Induction ratio adjustment function activated.

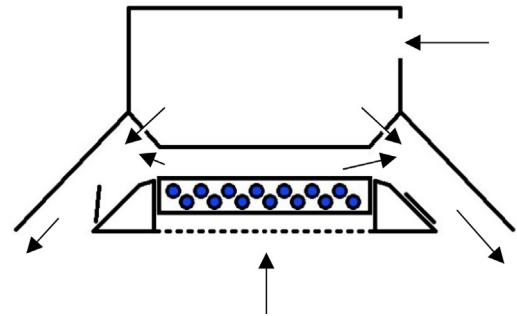


Fig. 3. Induction ratio adjustment function on to the left and off to the right.

2.2. Comparison of three methods

In order to see whether the compliance of the investigated methods was affected by the operating conditions the comparison was made at different primary air flows, chilled water temperatures and room temperatures. The desired room temperature was achieved by adjusting the internal heat gain. Additionally, in one case an induction ratio adjustment function was activated. This is a function provided in active chilled beams produced by Halton Oy in order to enhance flexibility in modern office environment [20]. The cases are declared in Table 1.

Fig. 3 illustrates the induction ratio adjustment function of one supply air outlet. In case 2, however, the function was activated in both supply air outlets.

The primary air temperature was kept at 20 °C in all cases and the exhaust air fan was controlled to match the primary air flow. The three investigated methods are described in the following.

2.2.1. Air velocity

By traversing a hot-wire anemometer in a dense grid in the induced air stream under the chilled beam the induced air flow rate could be calculated. After ensuring that the velocity profile was symmetrical, measurements were made in 90 points only under one quarter of the beam. The grid of measurement points was denser close to the edges and sparser in the middle (where the velocity gradients were smaller). Velocities between the points were estimated by cubic spline interpolation. Smoke was used to visualize the air flow under the surface between induced air inlet and supply air outlet in order to determine how much of this upwards moving room air that was entrained by the supply air even before it reached the active chilled beam. The resulting velocity profile from measurements of one case is presented in Fig. 4.

Additionally, a simplified version of this method was used to study the influence of temperatures of chilled water and room air at low primary air flows. The simplified version included a single-point air velocity measurement in a flow hood covering about a fourth of the induced air flow.

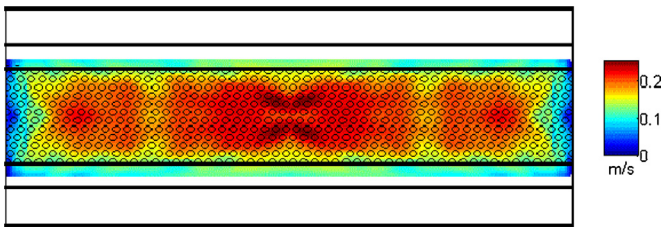


Fig. 4. Measured velocity profile of the induced air.

2.2.2. Modified capacity

Both the capacity method and the temperature method presented in previous section suffer from the difficulties of measuring the temperature of the induced air downstream the coil. But by combining the two methods it is possible to find an expression for IR without that problem. The capacity method (Eq. (1)) and the temperature method (Eq. (2)) are combined into the modified capacity method (Eq. (3)).

$$IR = \frac{\dot{m}_w \cdot c_{p,w} \cdot (t_{w,out} - t_{w,in})}{\dot{m}_p \cdot c_{p,a} \cdot (t_r - t_{i,out})} \quad (1)$$

$$IR = \frac{t_p - t_s}{t_s - t_{i,out}} \quad (2)$$

$$IR = \frac{t_s - t_p}{t_r - t_s} + \frac{\dot{m}_w \cdot c_{p,w} \cdot (t_{w,out} - t_{w,in})}{\dot{m}_p \cdot c_{p,a} \cdot (t_r - t_s)} \quad (3)$$

\dot{m} is mass flow, c_p is specific capacity and t temperature. Index w is chilled water, p is primary air, s is supply air, i, out is induced air downstream the coil, and r is room air (see Fig. 1).

Supply air temperature is the average of four sensors positioned at one and two thirds of the length of the beam in each supply air outlet slot. Room temperature is the average of two sensors positioned 25 cm under the beam at one and two thirds of the length of the beam. It is assumed that this temperature represents the air-side inlet temperature. All air temperature sensors were radiation shielded.

Sampling rate of recorded measurements was one per minute. Presented values are the average of the last 30 recordings when steady state conditions were obtained. Steady state conditions were considered to have been obtained when the standard deviation of the last 60 recorded measurements of the room temperature was below 0.055 °C.

2.2.3. Tracer gas

Increasing the concentration of carbon dioxide (CO₂) in the room made it possible to calculate the IR by simultaneously measuring the concentration of CO₂ in the induced air, in the primary air and in the supply air. Before measuring the supply air CO₂-concentration, both the supply and induced air sensors were positioned in the induced air stream in order to verify the calibration. Result from the one of the cases is presented in Fig. 5.

2.3. Influence of operating conditions

Findings from the comparison of methods were utilized in order to enhance the modified capacity method. The enhanced version was then used to study the influence of the operating conditions in detail. Two levels of internal heat gain (450 and 765 W), four chilled water supply temperatures (16, 18, 20 and 22 °C), two chilled water flow rates (2.0 and 2.9 l/min) and three primary air flows (15, 25 and 35 l/s) was combined and formed 48 cases of operating conditions.

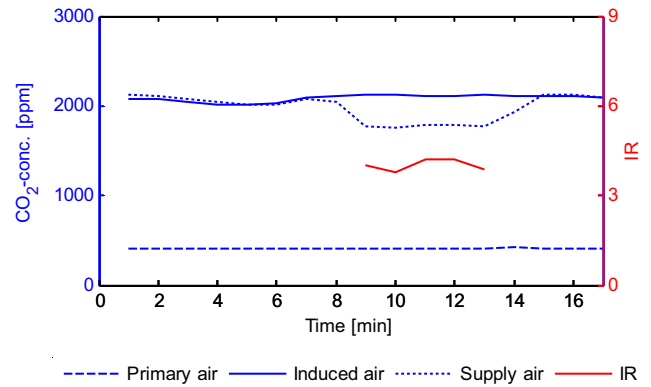


Fig. 5. Measured concentrations of CO₂ and determined IR using the tracer gas method.

Table 2

Determined values of IR of the 8 cases.

	Velocity method	Modified capacity method	Tracer gas method	Average method
1	5.1	6.2	5.5	5.6
2	3.1	4.3	4.0	3.8
3	5.2	6.2	5.1	5.5
4	4.7	6.0	4.7	5.1
5	5.6	6.3	4.5	5.5
6	4.8	6.0	5.1	5.3
7	5.3	6.0	7.1	6.1
8	4.8	6.4	6.3	5.8
Avg.	4.8	5.9	5.2	5.3

3. Results

The results are divided into one section where three different measurements methods are compared and one section where primarily one method is used to investigate the influence of operating conditions. However, also the first section includes different sets of operating conditions. The first section includes 8 sets of operating conditions while the second section includes 48.

3.1. Comparison of three methods

The determined values of IR are presented in Table 2.

As can be seen in Table 2, the modified capacity method gives the highest IR in all cases but one, and higher IR than the velocity method in all cases. Results from the tracer gas method diverge more randomly while the difference between the modified capacity method and the velocity method is more consistent.

One simplification in the modified capacity method is that the influence of radiation is omitted. The difference between the modified capacity method and the velocity method is bigger in cases with more radiation and vice versa. Therefore, it is reasonable to suggest that the neglect of radiation leads to overestimation of the IR and is a major source to the difference between the two methods.

Hence, in order to take radiation into account, a radiation term was added to Eq. (3), see Eq. (4).

$$IR = \frac{t_s - t_p}{t_r - t_s} + \frac{\dot{m}_w \cdot c_{p,w} \cdot (t_{w,out} - t_{w,in}) - A \cdot \varepsilon \cdot \sigma \cdot (T_r^4 - T_w^4)}{\dot{m}_p \cdot c_{p,a} \cdot (t_r - t_s)} \quad (4)$$

A is the area of the beam, ε the emissivity, σ the Stefan-Boltzmann constant, T_r the room air temperature expressed in kelvin and T_w the average of chilled water supply and return temperature expressed in kelvin. This equation involves two simplifications. Firstly, the temperature of the surfaces absorbing radiative heat is in reality higher than the temperature of the chilled water, primarily

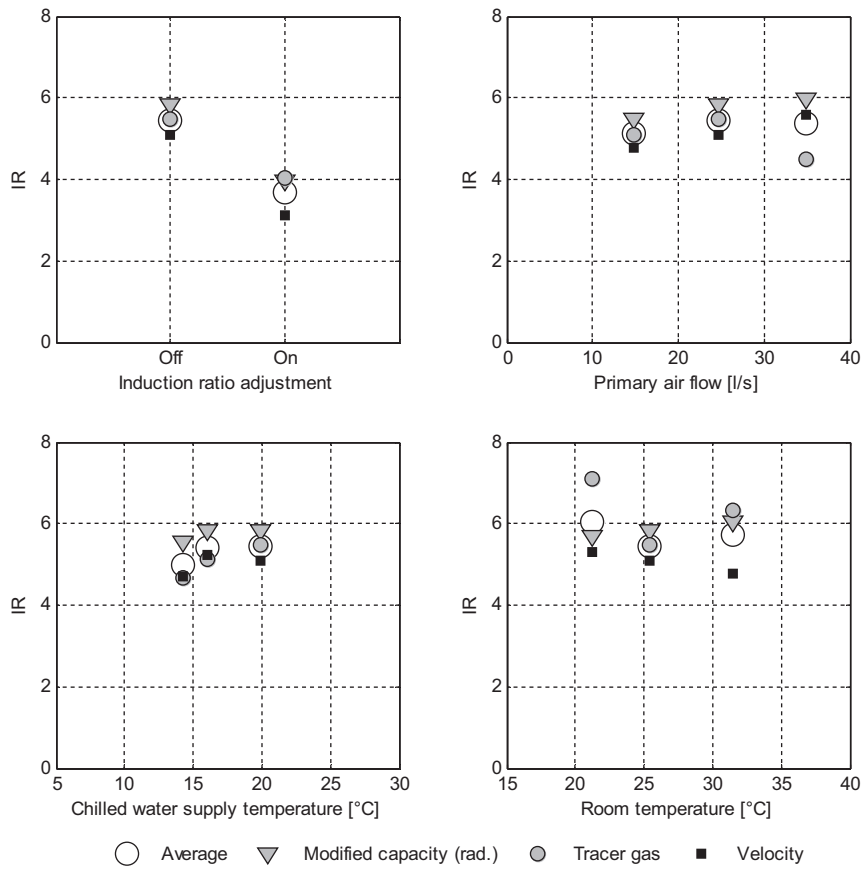


Fig. 6. Determined values of IR plotted against the operating conditions.

because of the grille positioned under the coil. Secondly, the temperatures of the surfaces radiating heat are higher than the room air temperature, definitely the surfaces of the dummies but also surfaces of walls and floor. To some extent, these simplifications may cancel each other out. This approach results in radiative load factors of 6–11% in the eight cases. Radiative load factor being defined as heat transferred by radiation divided by all heat transferred to the chilled water.

IR values from the tracer gas method, velocity method and capacity method (Eq. (4)) are presented in Fig. 6.

As seen in the top left part of Fig. 6, the induction ratio adjustment function decreased the IR by approximately 30% according to all three methods. Although results from the tracer gas method are in line with the other methods in general, some major discrepancies occur. The velocity method and the modified capacity method give similar results, but not in the case with the high room air temperature.

3.2. Influence of operating conditions

Following results are obtained by using Eq. (4). Fig. 7 shows the calculated IR as a function of the investigated parameters.

As seen in the top left part of Fig. 7, the chilled water flow rate has a very small influence on the IR. Regarding the primary air flow, higher IR is obtained at an intermediate air flow, while both higher and lower air flow impair the IR. Higher chilled water temperature gives higher IR (0.08 K^{-1} on average), while the influence of internal heat gain can be used to draw conclusions about the influence of room air temperature. Fig. 8 shows the IR values plotted against the room air temperature. The lines connect points with internal heat gain as the only difference. Hence, the slope of the lines shows the influence of room air temperature but cleared from influence

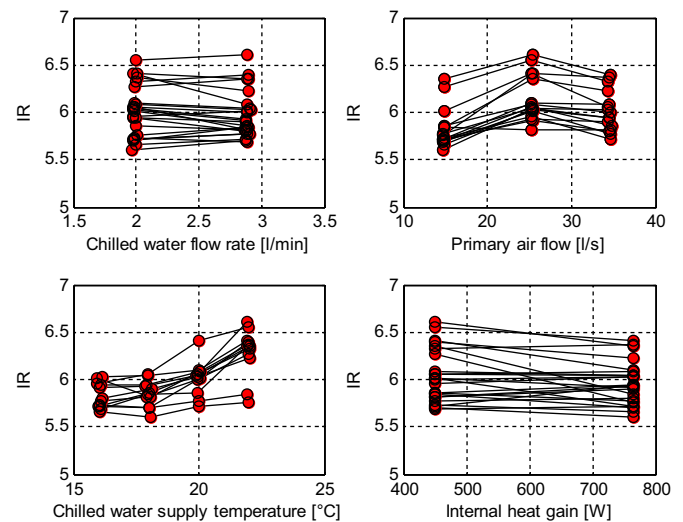


Fig. 7. Determined values of IR plotted against the operating conditions. Points connected by lines have the same operating conditions except the one parameter on the x-axis.

of chilled water temperature, chilled water flow rate and primary air flow rate.

As can be seen in Fig. 8, no unequivocal conclusion can be drawn regarding the correlation between room air temperature and IR. However, the primary air flow seems to influence whether the room air temperature is positively or negatively correlated to the IR. At low primary air flow, increased room temperature has the same influence as decreased chilled water temperature (on average -0.06 K^{-1} at 15 l/s). However, at high primary air flows the

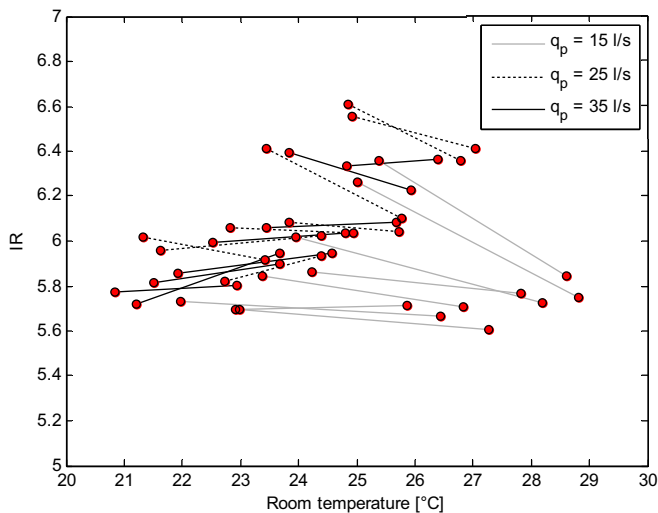


Fig. 8. Determined values of IR plotted against room temperature. Lines connect points with internal heat gain as the only difference.

opposite occurs, higher room air temperature gives higher IR (on average 0.02 K^{-1} at 35 l/s).

3.2.1. Single-point air velocity measurement

Results presented in Fig. 9 were produced by measuring air velocity in a flow hood positioned in the induced air flow under the chilled beam. The measured air velocity is divided by the primary air flow in order to obtain a value comparable to the IR.

Comparing the circles in Fig. 9 verifies that an increased chilled water temperature gives higher IR. Comparing the squares verifies that a decreased room air temperature gives higher IR. These buoyant phenomena becomes more apparent at low flows of primary air since the fan-driven forces diminishes. However, these results should not be used to draw conclusions about the correlation between primary air flow and IR. Only a fraction of the induced air flow is covered by the flow hood and the ratio of air flowing through and beside the flow hood may vary as a function of the primary air flow.

3.3. Uncertainty of results

The maximum and average uncertainties of the IR values presented in section 3.2 are estimated to be 7.6% and 4.8% respectively. This includes random uncertainties (estimated from statistical analysis of the measured data) as well as systematic uncertainties (estimated from specifications declared by producers of the instruments). The systematic uncertainties are about four times larger than the random uncertainties. This indicates that even though the actual determined values of IR are associated with a notable uncertainty, the correlations and relative differences between them are less uncertain.

The uncertainty is to a large extent determined by the primary air flow since lower air flows give smaller pressure differences which is associated with higher relative uncertainties. The uncertainties of cases with the high (35 l/s) primary air flow ranged between 2.7% and 4.5% while between 5.4% and 7.6% for cases with the low (15 l/s) primary air flow. The estimated uncertainties presented here however, do not include systematic uncertainties associated with the assumptions of radiation (e.g. emissivity, area and the simplifications regarding temperatures).

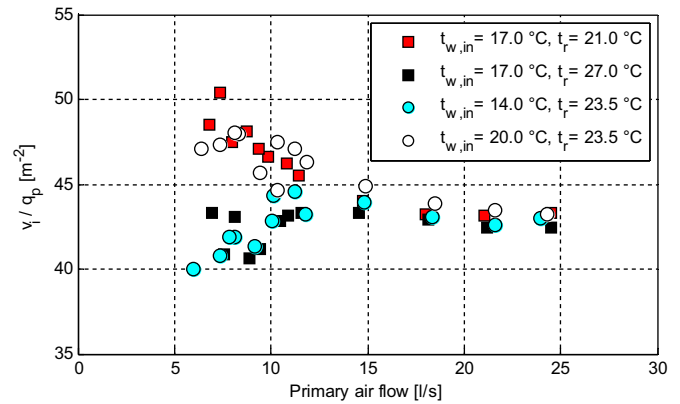


Fig. 9. Measured induced air velocity (v_i) divided by primary air flow (q_p) at different temperatures of chilled water and room air, plotted against the primary air flow.

4. Discussion and conclusions

Generally, the modified capacity method gives higher IR than the other methods. This is in accordance with findings by Ruponen and Tinker [6]. They found that the capacity method overestimated the IR by 29% on average and they suggested that it was caused by the positioning of the temperature sensor downstream the coil. In the modified capacity method presented in this study, the positioning problem was avoided and the average overestimation was reduced to 24% compared to the velocity method. By also taking radiation into account the difference between the methods was down to 15%.

This paper presents two new methods of measuring the IR, the modified capacity method and the tracer gas method. Although the results from the tracer gas method were less consistent than the other methods, it may still be considered a suitable option when doing on-site IR measurements if simplicity is prioritized while accuracy is secondary.

The velocity method showed a trend of decreasing IR at higher room temperature while the modified capacity method showed the opposite trend. Several corrections of the capacity method equation were investigated in order to find the cause. However, none gave better overall correlation than the used one. Investigated corrections were: assuming incomplete mixing of induced and primary air, temperature increase of primary air between sensor and nozzle, increased radiation due to hot dummies and decreased radiation due to the grille being warmer than the coil.

The results of the work behind this paper indicate that a higher chilled water temperature gives higher IR. In contrast, the correlation between room air temperature and IR seems more complex. The warm room air moves upwards and cools in the cold coil of the chilled beam. On the one hand, warmer air slows down more when it cools down in the coil, on the other hand warmer air is lighter and more easily elevated by the inductive force. Results presented in this paper indicate that the first phenomenon dominates at low air flows while the second one dominates at high air flows. In order to take buoyant forces into account Livchak and Lowell [5] suggested expressing the flow of secondary air as a function of the difference between room air temperature and chilled water temperature. The results from this study indicate that not only the difference but also the levels of the temperatures should be considered, especially when the air flow rate is high.

Traditionally, the IR is often expressed as a function of the primary air flow. Results presented in this paper indicate that the chilled water temperature is of similar importance. One could of course argue that the influence is unimportant in systems with constant chilled water supply temperature. However, the chilled water supply temperature is seldom constant. In traditional systems, it is

varied due to dew point compensation and in high temperature systems without control of chilled water flow rate, it may be varied in order to control the cooling capacity.

Results regarding the correlation between room air temperature and IR is not considered consistent enough to allow a generalization. Consequently, this is a topic recommended for further investigations. Improved knowledge on this topic may be useful to enhance the self-regulating characteristics of active chilled beams. This study is limited to one design of active chilled beams. Other designs, e.g. where the air passes the coil horizontally, would result in other conclusions.

Acknowledgement

This paper is a result of the research project *Self-Regulating Active Chilled Beam Systems*. The project is funded by the Construction Industry Organisation for Research and Development (SBUF) in Sweden.

References

- [1] J. Gräslund, Kompressorfri kyla i energieffektivt kontor, *Energi Miljö* 86 (11) (2015) 48–51.
- [2] F. Domínguez-Muñoz, J.M. Cejudo-Lopez, A. Carrillo-Andrés, Uncertainty in peak cooling load calculations, *Energy Build.* 42 (7) (2010) 1010–1018.
- [3] L. Peeters, I. Beausoleil-Morrison, A. Novoselac, Internal convective heat transfer modeling: critical review and discussion of experimentally derived correlations, *Energy Build.* 43 (9) (2011) 2227–2239, <http://dx.doi.org/10.1016/j.enbuild.2011.05.002>.
- [4] J. Le Dréau, P. Heiselberg, R.L. Jensen, Experimental investigation of the influence of the air jet trajectory on convective heat transfer in buildings equipped with air-based and radiant cooling systems, *J. Build. Perform. Simul.* 8 (5) (2015) 312–325, <http://dx.doi.org/10.1080/19401493.2014.938121>.
- [5] A. Livchak, C. Lowell, Don't turn active beams into expensive diffusers, *ASHRAE J.* 54 (4) (2012) 52–60.
- [6] M. Ruponen, J.A. Tinker, A novel method to measure the air entrainment ratio of an active chilled beam, *Int. J. Vent.* 7 (4) (2008) 299–308.
- [7] Z. Guan, C. Wen, Geometric optimization on active chilled beam terminal unit to achieve high entrainment efficiency, *Appl. Therm. Eng.* 98 (2016) 816–826, <http://dx.doi.org/10.1016/j.applthermaleng.2015.12.092>.
- [8] C. Chen, W. Cai, K. Giridharan, Y. Wang, A hybrid dynamic modeling of active chilled beam terminal unit, *Appl. Energ.* 128 (2014) 133–143.
- [9] J.S. Hyun, J.Y. Kim, H.J. Shin, J.S. Kim, Induction performance design of chilled beam system, Paper Presented at the ACRA 2014 – Proceedings of the 7th Asian Conference on Refrigeration and Air Conditioning (2014).
- [10] K.N. Rhee, M.S. Shin, S.H. Choi, Thermal uniformity in an open plan room with an active chilled beam system and conventional air distribution systems, *Energy. Build.* 93 (2015) 236–248, <http://dx.doi.org/10.1016/j.enbuild.2015.01.068>.
- [11] G. Cammarata, G. Petrone, A numerical investigation on active chilled beams for indoor air conditioning, in: B. Nilsson (Ed.), Paper Presented at the COMSOL Conference (2008).
- [12] H. Freitag, P. Mathis, D. Müller, Influence of thermal Boundary Conditions on the Entrainment Behavior of an Active Chilled Beam. Paper presented at the 12th REHVA World Congress: volume 5. Aalborg: Aalborg University, Department of Civil Engineering, in: Heiselberg P. K (eds) 2016.
- [13] C. Chen, W. Cai, Y. Wang, C. Lin, L. Wang, Operating characteristics and efficiencies of an active chilled beam terminal unit under variable air volume mode, *Appl. Therm. Eng.* 85 (2015) 71–79, <http://dx.doi.org/10.1016/j.applthermaleng.2015.03.016>.
- [14] A. Maccarini, G. Hultmark, A. Vorre, A. Afshari, N.C. Bergsøe, Modeling of active beam units with Modelica, *Build. Simulat.* (2015) 1–8.
- [15] M. Ruponen, J.A. Tinker, Novel method for measuring induction rates, Paper Presented at the 10th International Conference on Air Distribution in Rooms (2007).
- [16] H. Freitag, D. Müller, Investigation of airflow effects in induction beams, Paper Presented at the 12th International Conference on Air Distribution in Rooms (2011).
- [17] C. Chen, W. Cai, Y. Wang, C. Lin, Further study on the heat exchanger circuitry arrangement for an active chilled beam terminal unit, *Energy Build.* 103 (2015) 352–364, <http://dx.doi.org/10.1016/j.enbuild.2015.07.001>.
- [18] BS 4954-1, Testing and Rating Induction Units for Air Distribution Systems ?Part 1, British Standards Institution, London.U.K, 1973.
- [19] M.T. Ruponen, Operation and Thermal Comfort Provision Using Induction Units, University of Leeds, 2009.
- [20] R. Kosonen, M. Virta, H. Oy, *Taking flexibility into account in designing beam systems*, in: Paper Presented at the 9th Federation of European Heating and Air-Conditioning Associations World Congress, Helsinki, 2007.

A Thermal Model of an Active Chilled Beam

Peter Filipsson^{1,2}, Anders Trüschel¹, Jonas Gräslund^{1,3}, Jan-Olof Dalenbäck¹

filipssp@chalmers.se (corresponding author)

anders.truschel@chalmers.se

jonas.graslund@skanska.se

jan-olof.dalenback@chalmers.se

¹ Division of Building Services Engineering, Department of Civil and Environmental Engineering, Chalmers University of Technology, 412 96, Gothenburg, Sweden

² CIT Energy Management AB, 412 88, Gothenburg, Sweden

³ Skanska Commercial Development Nordic AB, 112 74, Stockholm, Sweden

Nomenclature

A	area [m ²]		
APE	Absolute percentage error [%]	c_p	specific heat capacity [J/kgK]
C	heat capacity rate [W/K]		
$C_{1,2,3,4,5,6,7}$	empirical constants		
D	diameter [m]		
f	Darcy friction factor [-]		
h	convective heat transfer coefficient [W/m ² K]		
IR	Induction ratio [-]		
K	empirical constant		
k	thermal conductivity [W/mK]		
\dot{m}	mass flow rate [kg/s]		
n	empirical constant		
NTU	number of transfer units [-]		
Nu	Nusselt number [-]		
P	cooling capacity [W]		
Pr	Prandtl number [-]		
q	volumetric flow rate [m ³ /s]		
Re	Reynolds number [-]		
T	temperature [K]		
u	mean fluid velocity [m/s]		
U	overall heat transfer coefficient [W/m ² K]		
ε	effectiveness, emissivity [-]		
σ	Stefan-Boltzmann constant [W/m ² K ⁴]		
ρ	density [kg/m ³]		
μ	dynamic viscosity [Ns/m ²]		
ν	kinematic viscosity [m ² /s]		
<i>Subscripts</i>			
a	air, air-side		
as	air-side surface		
D	diameter		
e	exhaust air		
i	inside		
in	inlet		
m	measured		
min	minimum		
max	maximum		
out	outlet		
p	projected		
pri	primary air		
r	ratio, room		
s	supply air		
sec	secondary air		
sim	simulated		
tot	total		
w	water, water-side		

59 **ABSTRACT**

60 Active chilled beams (ACBs) have gained increased recognition as a feasible technology for comfort
61 cooling during the last decades. One of the advantages with such systems is utilization of high
62 temperature cooling. This provides exergetic benefits and also reduces the need for individual room
63 control. However, individual room control normally serves as compensation for the safety margin applied
64 when dimensioning the cooling systems. Therefore, the absence of individual room controls calls for
65 accurate dimensioning tools.

66 This paper presents a model to be used to calculate cooling capacities of ACBs. The model is based on
67 NTU analysis and is a hybrid of first principles and empirical data in order to ensure high accuracy
68 without requiring extensive measurements for model calibration. This is the first ACB model that
69 explicitly captures the influence of buoyant forces acting on the air passing the chilled coil in the beam.
70 Output from the model also includes temperature and flow of supply air.

71 The model shows good compliance with measured data in a wide range of operating conditions (average
72 error of 1.7% if six cases is used for model calibration). The model can be appropriately implemented in
73 building performance simulation tools, thus improving the design of ACB systems.

74 **Keywords:** active chilled beams, model, NTU, heat transfer

75 **Highlights:**

- 76
- Requires very few cases for model calibration.
 - 77 • Provides accurate results in a wide range of operating conditions.
 - 78 • Determines cooling capacity as well as temperature and flow of supply air.

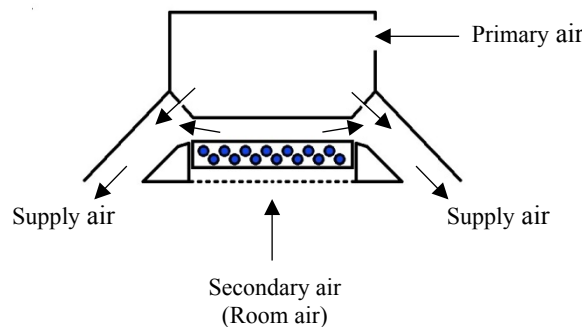
79 **1 Introduction**

80 Energy efficient technologies for heating and cooling in buildings are assumed to play a crucial role in
81 switching to sustainable societies [1]. However, while the demand for space heating in the EU and the
82 OECD countries is not expected to grow any further, the demand for space cooling is expected to rise
83 substantially [2], recent predictions indicate a 100% increase in global space cooling demand between
84 2005 and 2030 [3]. The growing demand is driven by intensification of urban heat islands (UHI) [4],
85 climate change, increased thermal comfort requirements, more glazed facades, higher internal loads and,
86 in cold regions, by more insulated building envelopes [5]. Furthermore, comfort cooling is strongly
87 correlated to income and will therefore increase very dramatically in developing countries [6]. While
88 space heating demand benefits from global warming and UHI-intensification, the opposite applies to
89 space cooling demand which becomes self-perpetuating if cooling is produced from fossil fuels and with
90 conventional heat emitting chillers. Sustainable space cooling technologies are urgently needed in order
91 to avoid this scenario.

92 **1.1 Active chilled beams**

93 A good example of energy efficient technology for space cooling is the use of active chilled beams
94 (ACBs). ACBs have gained increased popularity the last decades due to favorable performance regarding
95 energy efficiency, thermal comfort and economy.

96 The operation of a very common type of ACB is illustrated in Figure 1. Primary air is provided from an
97 air handling unit while chilled water is circulated through a cooling coil inside the ACB. The primary air
98 enters the room via a pressure plenum and several nozzles along the beam. The high primary air velocity
99 generated by the nozzles induces secondary air (room air) that cools down as it passes the coil. The mixed
100 air is then discharged into the room through slots along both long sides of the beam.



101
102
103 *Figure 1 Schematic diagram of an active chilled beam*

104 The secondary air flow rate divided by the primary air flow rate is referred to as the induction ratio (IR).
105 The flow of chilled water is usually controlled as a function of the room air temperature in order to match
106 the cooling capacity with the actual demand.

107 A key opportunity with ACBs is utilization of high temperature cooling. This provides major benefits
108 such as increased use of free cooling, better performance of chillers, reduced risk of condensation
109 (reduced latent load), reduced thermal losses in the chilled water distribution system and less need for
110 individual room control. Gräslund [7] presents a high temperature ACB system without chillers, room
111 thermostats and pipe insulation. The water is chilled in boreholes and by preheating incoming outdoor
112 air (when needed). Due to the self-regulating characteristic of high temperature cooling, there are no
113 individual room control of the chilled water flow rate.

114 In the absence of individual room control systems, more accurate simulation models are required when
115 dimensioning the cooling capacity. Traditionally, worst-case scenarios or crude safety margins have been
116 used when designing comfort cooling systems. The safety margins are compensated for by the room
117 control and the only consequence is oversized equipment. In a system without individual room control
118 on the other hand, oversized equipment will impact the room air temperature.

119 A very common way of modelling the cooling capacity of ACBs are prescribed by the European standard
120 EN 15116 [8]. The cooling capacity, P_w , is expressed as a power function of the driving temperature
121 difference, ΔT , according to Equation 1.

$$122 \quad P_w = K \cdot \Delta T^n \quad \text{(Equation 1)}$$

123 The temperature difference between room air, T_r , and the chilled water, is defined according to

$$124 \quad \Delta T = T_r - \frac{T_{w,in} + T_{w,out}}{2} \quad \text{(Equation 2)}$$

125 where $T_{w,in}$ and $T_{w,out}$ is the chilled water inlet and outlet temperatures respectively. K and n are
126 empirical coefficients that for a specific beam need to be determined as functions of primary air and
127 chilled water flow rates. These coefficients may then be used to simulate ACBs in building performance
128 simulation software [9]. A comprehensive review of how ACBs are modelled in five common building
129 simulation software are found in Betz et al. [10].

130 A number of more sophisticated models have been presented in the recent years. Chen et al. [11]
131 concluded that their model performed satisfactory both during static and dynamic operation. They noted
132 that the model was useful in real-time control and optimization applications, e.g. to avoid condensation,
133 but also called for simplifications of the complexity of the model. Livchak and Lowell [12] presented a
134 set of equations describing the cooling capacity of ACBs applicable in building performance simulation
135 software. Coefficients used in the equations were said to be available from manufacturer's capacity tests.
136 However, Maccarini et al. [13] concluded that manufacturers generally do not provide enough data to
137 derive the coefficients. Maccarini et al. [13] made some adjustments to the empirical equations proposed
138 by Livchak and Lowell [12] and presented an ACB model developed with the programming language
139 Modelica. The model was validated both in cooling and in heating mode and it was concluded that it
140 corresponded closely with the actual operation. De Clercq et al. [14] used the NTU (number of transfer
141 units) method to model heating and cooling capacities of ACBs. The results showed very good
142 compliance with measured data.

143 Due to buoyant forces, the secondary air flow rate, and consequently the IR, is influenced by the
144 temperatures of the chilled water and the room air. This is to some extent taken into account in all ACB
145 models. In some models explicitly, where the IR is expressed as a function of the difference between the
146 two temperatures, otherwise implicitly, by affecting the empirical coefficients describing the cooling
147 capacity as a function of the difference between the two temperatures. However, results from Filipsson
148 et al. [15] indicates that the chilled water temperature is more influential than the room air temperature.
149 This finding suggests that the IR may be expressed more accurately as a function of the chilled water
150 temperature rather than the difference between room air and chilled water temperature. This paper
151 presents the first model of an ACB taking that finding into account.

152 **1.2 Objectives**

153 The objectives of the work presented in this paper is to develop a thermal model of an active chilled
154 beam. The model should be a fair trade-off between accuracy, practicability and transparency while
155 providing cooling capacity as well as supply air temperature and flow rate as output.

156 2 Method

157 The work presented in this paper may be divided into three parts: derivation of the model, calibration of
158 the model and validation of the model. It can also be divided into three parallel parts: advanced model,
159 simplified model and operation at nonturbulent flow of chilled water.

160 2.1 Model

161 The total cooling capacity, P_{tot} , of an active chilled beam is the sum of cooling from the primary air,
162 P_a , and cooling from the chilled water in the coil, P_w , according to Equation 3.

$$163 P_{tot} = P_a + P_w$$

164 (Equation 3)

165 Cooling from the primary air is calculated as

$$166 P_a = q_{pri} \cdot \rho_a \cdot c_{p,a} \cdot (T_{pri} - T_e)$$

167 (Equation 4)

168 where q_{pri} is the primary air flow, ρ_a and $c_{p,a}$ are the density and specific heat of the air and T_{pri} and
169 T_e are the temperatures of primary air and air exhausted from the room.

170 Cooling from the chilled water can be expressed as

$$171 P_w = \dot{m}_w \cdot c_{p,w} \cdot (T_{w,out} - T_{w,in}) \quad (\text{Equation 5})$$

172 where \dot{m}_w and $c_{p,w}$ are the mass flow rate and specific heat of the chilled water and $T_{w,out}$ and $T_{w,in}$
173 are the chilled water outlet and inlet temperature respectively.

174 However, since the chilled water outlet temperature is generally unknown, this equation cannot be used
175 to model the cooling capacity and another approach is necessary. A commonly used approach in heat
176 exchanger analysis of situations where the outlet temperatures are unknown is the NTU method (often
177 also referred to as the effectiveness-NTU method). The NTU method introduces the effectiveness
178 parameter ε which is the ratio of the actual heat transfer rate to the theoretical maximum heat transfer
179 rate. Thus, the chilled water cooling capacity is expressed as

$$180 P_w = \varepsilon \cdot C_{min} \cdot (T_r - T_{w,in}) \quad (\text{Equation 6})$$

181 where C_{min} is the minimum heat capacity rate according to

$$182 \quad C_{min} = \min((\dot{m}_w \cdot c_{p,w}), (q_{sec} \cdot \rho_a \cdot c_{p,a})) \quad (\text{Equation 7})$$

183 where q_{sec} is the volumetric flow rate of secondary air.

184 The effectiveness, ε , is as a function of the dimensionless parameter NTU and the heat capacity rate ratio

185 $C_r = C_{min}/C_{max}$. The flow arrangement in the heat exchanger of an ACB is too complex to be expressed

186 with a simple analytical effectiveness-NTU correlation. Instead one must rely on empirical

187 approximations. The most common correlation used for cross-flow heat exchangers in HVAC-

188 applications is presented by Equation 8 [16].

$$189 \quad \varepsilon = 1 - \exp\left(\frac{1}{C_r} \cdot NTU^{0.22} \cdot (\exp(-C_r \cdot NTU^{0.78}) - 1)\right) \quad (\text{Equation 8})$$

190 However, Laskowski et al. [17] concluded that the following approximation is a more accurate

191 correlation when NTU is less than 3, which is the case in an ACB under normal operation.

$$192 \quad \varepsilon = \left(\frac{NTU}{1 + 1.1238 \cdot NTU} + e^{-NTU} - 1\right) \cdot C_r + 1 - e^{-NTU} \quad (\text{Equation 9})$$

193 Introducing UA as the product of heat transfer area and overall heat transfer coefficient, NTU is defined

194 as

$$195 \quad NTU = \frac{UA}{C_{min}} \quad (\text{Equation 10})$$

196 By neglecting the conductive heat transfer resistance in the coil the UA can be calculated as a function

197 of the convective heat transfer properties of the air- and water-side ($(hA)_a$ and $(hA)_w$) according to

198 Equation 11.

$$199 \quad UA = \frac{1}{\frac{1}{(hA)_a} + \frac{1}{(hA)_w}} \quad (\text{Equation 11})$$

200 Calculation of the convective heat transfer on the water-side at turbulent flow is quite straightforward

201 and well-established. The convective heat transfer coefficient on the water-side is related to the Nusselt

202 number (Nu_D) as

$$203 \quad (hA)_w = Nu_D \cdot \frac{k_w}{D_i} \cdot A_w \quad (\text{Equation 12})$$

204 where k_w is the thermal conductivity of the chilled water while D_i and A_w are the inner diameter and
 205 inner surface area of the coil pipes. According to Incropera et al. [18], the Nusselt number is calculated
 206 as a function of the Darcy friction factor, f , the Reynolds number, Re_D , and the Prandtl number, Pr_w ,
 207 according to

$$208 \quad Nu_D = \frac{(f/8) \cdot (Re_D - 1000) \cdot Pr_w}{1 + 12,7 \cdot \sqrt{(f/8)} \cdot (Pr_w^{2/3} - 1)}$$

209 (Equation 13)¹

210 where the Darcy friction factor is determined as

$$211 \quad f = (0,790 \cdot \ln(Re_D) - 1,64)^{-2} \quad (\text{Equation 14})^2$$

212 The Reynolds number for internal flow is defined as

$$213 \quad Re_D = \frac{u \cdot D_i}{\nu} \quad (\text{Equation 15})$$

214 where u and ν are the mean velocity and kinematic viscosity of the chilled water.

215 The convective heat transfer on the air-side is much more difficult to estimate since the geometry and
 216 airflow is more complex. Furthermore, the air-side is unfortunately the more important side, since that is
 217 where the major heat transfer resistance occur. Rabehl et al. [19] presents a technique where all geometric
 218 terms are lumped into two characteristic parameters, C_1 and C_2 , allowing the convective heat transfer
 219 coefficient on the air-side to be expressed as

$$220 \quad (hA)_a = C_1 \cdot k_a \cdot \left(\frac{\dot{m}_a}{\mu_a}\right)^{C_2} \cdot Pr_a^{0.36} \cdot \left(\frac{Pr_a}{Pr_{as}}\right)^{0.25} \quad (\text{Equation 16})$$

221 where k_a is the thermal conductivity of the air, \dot{m}_a is the mass flow rate of the air, μ_a the dynamic
 222 viscosity of the air, Pr_a is the Prandtl-number evaluated at the mean air temperature and Pr_{as} is the
 223 Prandtl-number evaluated at the surface temperature. Due to the inferior thermal resistance between
 224 chilled water and air-side surface, the temperature of the air-side surface is assumed to equal the mean

¹ Valid at Reynolds number between 3 000 and 10 000

² Valid at Reynolds number between 3 000 and 5 000 000

225 chilled water temperature. The mass flow rate of induced air passing the coil, \dot{m}_a , can be expressed as a
226 function of the induction ratio according to Equation 17.

$$227 \quad \dot{m}_a = IR \cdot q_{pri} \cdot \rho_a \quad (\text{Equation 17})$$

228 Depending on the purpose of the model, different trade-offs between complexity and inaccuracy may be
229 chosen. Filipsson et al [15] concluded that the induction ratio may be expressed accurately as a function
230 of the chilled water supply temperature and the primary air flow rate according to

$$231 \quad IR = C_3 + C_4 \cdot T_{w,in} + C_5 \cdot q_{pri} + C_6 \cdot T_{w,in} \cdot q_{pri} + C_7 \cdot q_{pri}^2$$

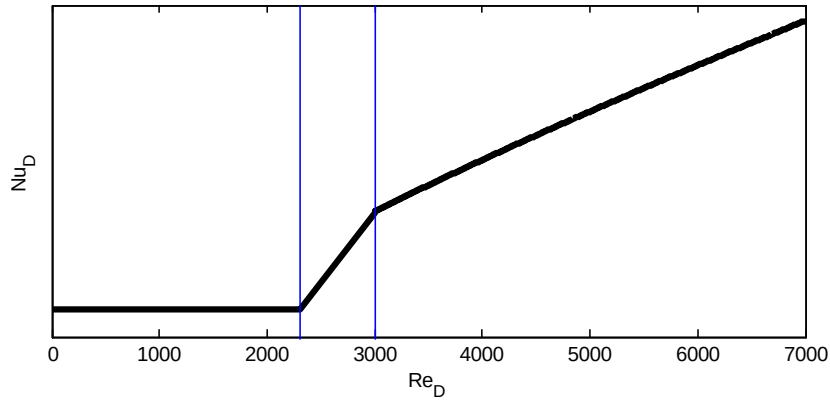
232 (Equation 18)

233 where C_3, C_4, C_5, C_6, C_7 are empirical constants estimated from results of measurements. In contrast
234 to Equation 18, a simpler model, where the induction ratio is constant and independent of operating
235 condition is also evaluated.

236 The characteristic parameters, C_1 and C_2 in Equation 16 can then be determined from measurement
237 results curve fits and the cooling capacity can finally be determined as a function of room air temperature,
238 primary air flow rate and flow rate and inlet temperature of chilled water.

239 **2.2 Operation at nonturbulent flow of chilled water**

240 Since Equation 13 and Equation 14 is valid only at turbulent flow ($Re_D > 3000$) some additional analysis
241 is required to make the model work at nonturbulent flow (laminar and transitional flow). At nonturbulent
242 flow, less established heat transfer theory is applicable at the same time as the water-side heat transfer
243 resistance becomes more influential. Consequently, one additional case is needed for calibration of the
244 model. According to Incropera et al. [18], the Nusselt number is a constant at fully developed laminar
245 flow and the critical Reynolds number corresponding to the onset of turbulence is 2300. In order to use
246 the model at nonturbulent flow, an approach according to Figure 2 is applied. It implies that the Nusselt
247 number is a constant at Reynolds numbers below 2300, that it is according to Equation 13 at above 3000
248 and linearly interpolated in between.



249

250

Figure 2 Modelled Nusselt number as a function of Reynolds number.

251

This expansion of the model requires only one additional measurement for calibration. The approach can

252

be divided into following two steps:

253

1. The air-side heat transfer is determined from measured cooling capacity in combination with well-established correlations for water-side heat transfer at turbulent flow.

254

255

2. By assuming that the air-side heat transfer properties are independent of flow rate of chilled

256

water, the water-side Nusselt number at laminar flow can be determined from measured cooling

257

capacity at laminar flow in combination with the previously determined air-side heat transfer

258

properties.

259

3 Measurements

260

The purpose of the measurements was twofold:

261

1. Calibration of the model. (Estimating the unknown parameters of equation 16 and 18 and the

262

water-side Nusselt number at laminar flow.)

263

2. Validation of the model. (Comparing measured results with results generated by the model.)

264

The flow rate of induced air, and consequently the IR, was determined from an energy balance using

265

the measured cooling capacity and air temperatures according to Equation 19. This approach was

266

analyzed by Filipsson et al. [15].

267

$$IR = \frac{T_s - T_{pri}}{T_r - T_s} + \frac{\dot{m}_w \cdot c_{p,w} \cdot (T_{w,out} - T_{w,in}) - A_p \cdot \varepsilon \cdot \sigma \cdot (T_r^4 - T_w^4)}{\dot{m}_p \cdot c_{p,a} \cdot (T_r - T_s)} \quad (\text{Equation 19})$$

268 T_w is the arithmetic mean of $T_{w,in}$ and $T_{w,out}$. T_s is the supply air temperature, ε and A_p is the
269 emissivity and projected area of the chilled beam and σ the Stefan-Boltzmann constant.

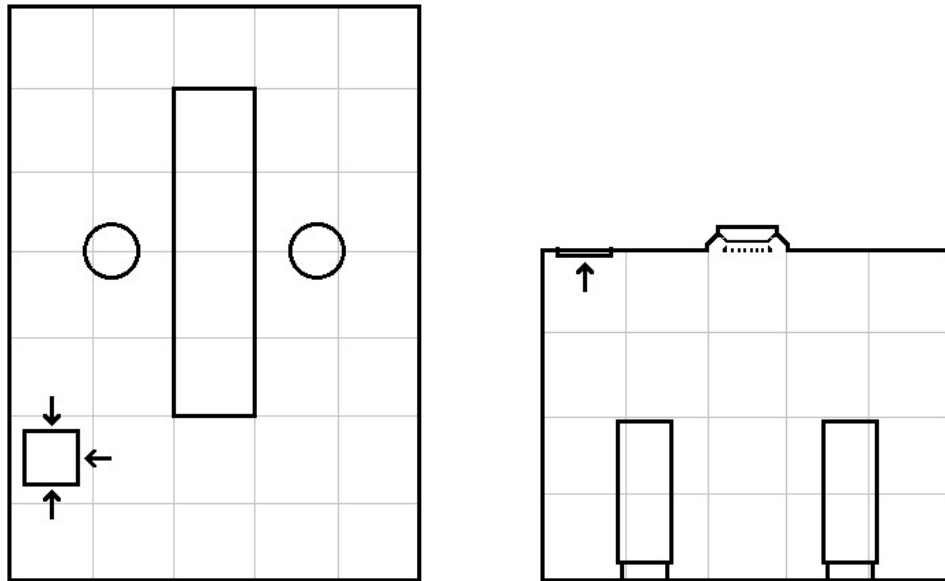
270 **3.1 Operating conditions**

271 Two levels of internal heat gain (450 and 765 W), four chilled water supply temperatures (16, 18, 20 and
272 22 °C), two chilled water flow rates (2.0 and 2.9 l/min) and three primary airflows (15, 25 and 35 l/s)
273 were combined and formed 48 sets of configurations (operating conditions), henceforth called cases. As
274 a consequence, the room air temperature varied between 21 and 29 °C. Additionally, 13 cases with
275 nonturbulent chilled water flow (0.4-1.5 l/min) were measured (all with internal heat gain of 765 W,
276 chilled water supply temperature of 18 °C and primary air flow of 25 l/s).

277 The primary air temperature was kept at 20 °C in all cases and the exhaust air fan was controlled to match
278 the primary air flow. Six of the cases were used for calibrating the model at turbulent water flow while
279 all 48 cases were used for model validation. The cases used for calibration included all three primary air
280 flows, only the highest and lowest chilled water temperatures, only the higher level of internal heat gain
281 and the lower chilled water flow rate. For the analysis of nonturbulent operation, one additional case was
282 used for calibration, while all 13 cases were used for validation.

283 **3.2 Experimental setup**

284 The measurements were carried out in a full-scale mockup of an office room. The internal dimensions of
285 the room were 3.0 m × 4.2 m × 2.4 m (width × length × height). The active chilled beam was positioned
286 in the suspended ceiling in the middle of the room and two thermal dummies (cooling load simulators)
287 were positioned on each side of the active chilled beam at half of the distance between the center and the
288 long side of the room. The temperature outside the room was controlled to not deviate more than 2 °C
289 from the temperature inside the room in order to minimize heat transfer through the envelope of the room.
290 The walls were made of 12 mm plasterboard attached on the inside of 100 mm expanded polystyrene.
291 The floor was made of 22 mm fiberboard on top of 6 mm plasterboard and 30 mm expanded polystyrene.



292

293 *Figure 3 Layout of the room and positions of active chilled beam, exhaust air terminal device and dummies. Top view to the*
 294 *left and front view to the right. Grey lines indicate a distance of 0.6 m.*

295 Measured supply air temperature is the average of four sensors positioned at one and two thirds of the
 296 length of the beam in each supply air outlet slot. Room temperature is the average of two sensors
 297 positioned 25 cm under the beam at one and two thirds of the length of the beam. All air temperature
 298 sensors were radiation shielded.

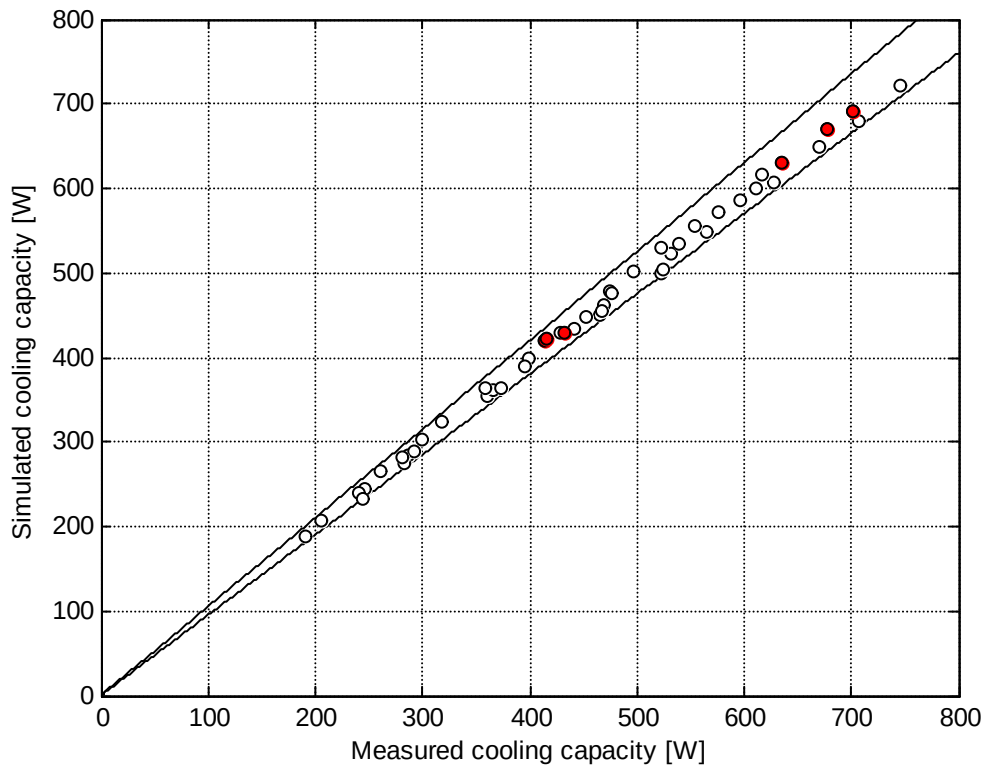
299 Sampling rate of recorded measurements was one per minute. Presented values are the average of the last
 300 30 recordings when steady state conditions were obtained. Steady state conditions were considered to
 301 have been obtained when the standard deviation of the last 60 recorded measurements of the room
 302 temperature was below 0.055 °C.

303 **4 Results**

304 The results are divided into advanced model, simplified model and operation at nonturbulent chilled
 305 water flow. The results are summarized in section 4.4.

306 **4.1 Advanced model**

307 The accuracy of the model is presented in Figure 4. Each circle represents a case. The red circles indicate
 308 the cases used to calibrate the model. The lines in the figure indicate simulation errors of $\pm 5\%$.



309

310 *Figure 4 Simulated and measured cooling capacity (advanced model). Red circles represent the cases used for calibration of*
 311 *the model. Lines show errors of ± 5 %.*

312 The accuracy of the model is presented as absolute percentage errors and are defined according to
 313 Equation 20 where P_m is the measured cooling capacity determined according to Equation 5 and P_{sim}
 314 is the simulated cooling capacity determined according to Equation 6.

315
$$APE = \left| \frac{P_m - P_{sim}}{P_m} \right| \quad \text{(Equation 20)}$$

316 The maximum error of the model is 4.7% and the average is 1.7%. Larger errors were found in cases
 317 with the higher flow rate of chilled water (2.3% on average), while cases with lower flow rate of chilled
 318 water had smaller errors (1.0% on average). This is probably because the unknown parameters of the
 319 model were estimated from cases with the lower flow rate. Using all 48 cases for calibration of the model
 320 improves the average error only to 1.6 %.

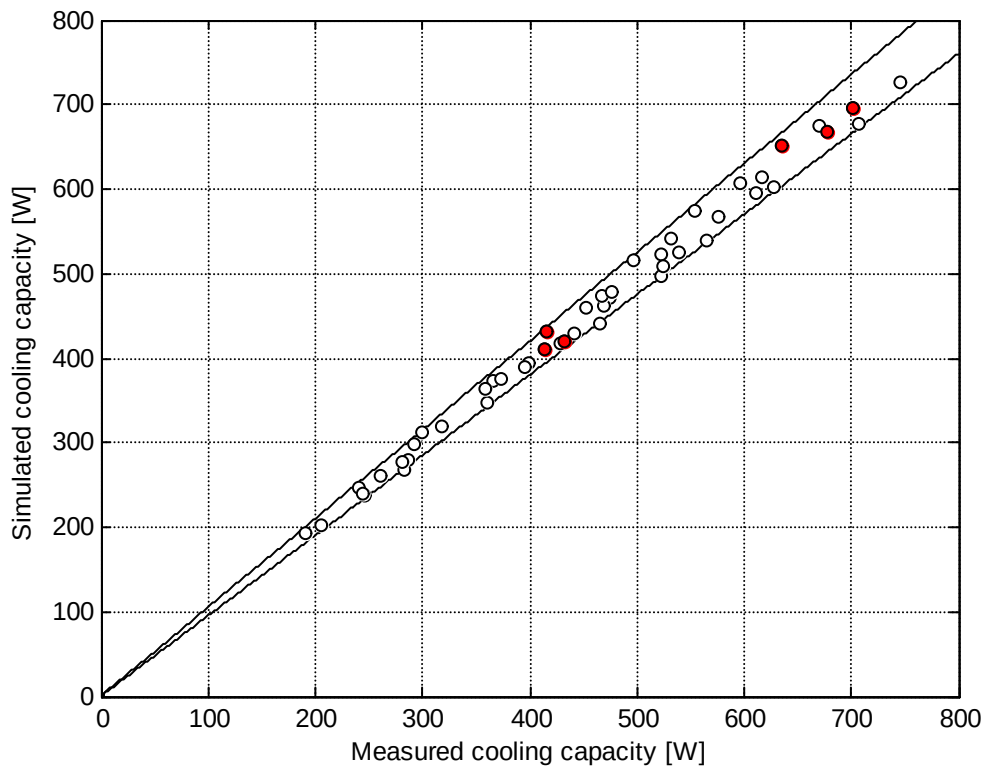
321 Since the model contains information about the IR, it can simulate the flow rate and temperature of supply
 322 air as well. The maximum and average absolute error of simulated supply air temperature are 0.2 and 0.1
 323 °C respectively. However, the temperature of the supply air of an ACB is not uniform. Air supplied in

324 the proximity of the chilled water inlet is colder than the air supplied in the proximity of the chilled water
325 outlet.

326 4.2 Simplified model

327 In the simplified model, the IR is constant and not affected by the operating conditions, i.e. substituting
328 Equation 18 with the average IR of the cases used for model calibration. This decreases the amount of
329 unknown parameters to be estimated from seven to three (C_1 , C_2 and IR). The maximum and average
330 error of this simplified model is 5.3% and 2.2% respectively. This is illustrated in figure 5.

331



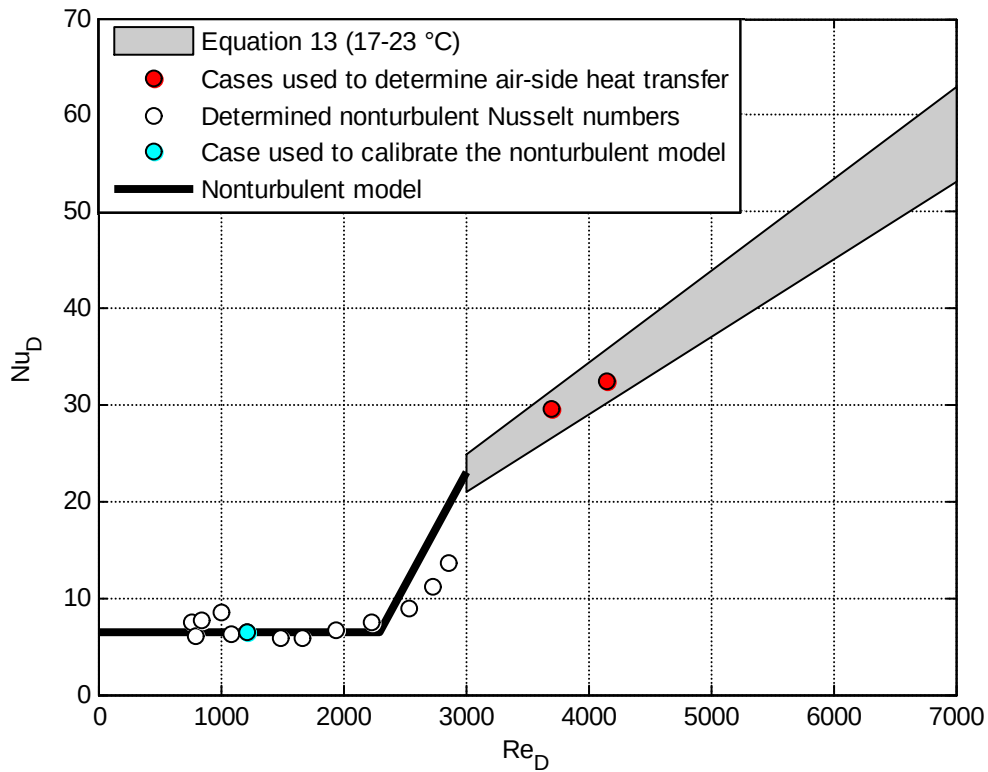
332

333 *Figure 5 Simulated and measured cooling capacity (simplified model). Red circles represent the cases used for calibration of*
334 *the model. Lines show errors of $\pm 5\%$.*

335 Since the simplified model does not contain information about how the IR depends on primary air flow
336 and chilled water supply temperature only two cases is required to calibrate the model (in order to
337 determine C_1 and C_2 while the average IR of the two cases is used as the constant IR). If using only two
338 cases for calibration, the average error worsen only to 2.7%.

339 **4.3 Operation at nonturbulent flow of chilled water**

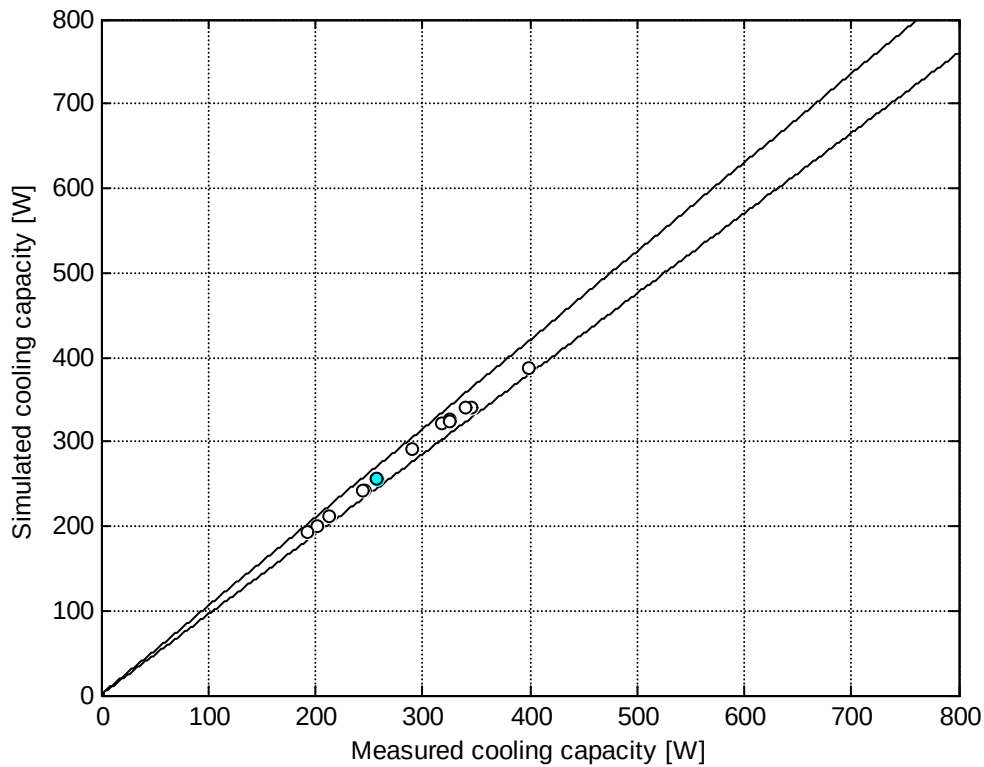
340 The determined Nusselt numbers of the 13 cases with nonturbulent flow of chilled water are presented
341 in Figure 6. The figure also presents the water side Nusselt numbers of the cases used to determine the
342 air-side heat transfer. Nusselt number of the nonturbulent model is plotted in order to visualize how well
343 the model corresponds to values determined from measurements.



344

345 *Figure 6 Water side Nusselt number as a function of water side Reynolds number.*

346 Since the water side heat transfer resistance is a minor part of the overall heat transfer resistance, errors
347 in water side Nusselt are not crucial for the determination of the cooling capacity. The accuracy of the
348 nonturbulent submodel is illustrated in Figure 7.



349

350 *Figure 7 Simulated and measured cooling capacity (at sub-turbulent flow of chilled water). The cyan colored square represent*
 351 *the case used for calibration of the model. Lines show errors of $\pm 5\%$.*

352 The average and maximum error of the nonturbulent submodel are 1.0% and 3.6% respectively. Since

353 the case for calibration is randomly chosen, presented percentages are averages of all possible choices.

354 The worst case choice results in average and maximum error of 1.4% and 4.7%

355 4.4 Summary of results

356 A summary of the accuracies of the model is presented in Table 1.

357 *Table 1 Summary of accuracies*

Flow type	Cases used for calibration	Cases used for validation	Induction ratio	Error (APE) [%]	
				Avg.	Max
Turbulent	48	48	$f(q_p, T_{w,in})$	1.6	4.5
Turbulent	48	48	Constant	2.0	4.5
Turbulent	6	48	$f(q_p, T_{w,in})$	1.7	4.7
Turbulent	6	48	Constant	2.2	5.3
Turbulent	2	48	Constant	2.7	6.7
Nonturbulent	2 + 1	13	$f(q_p, T_{w,in})$	1.0	3.6

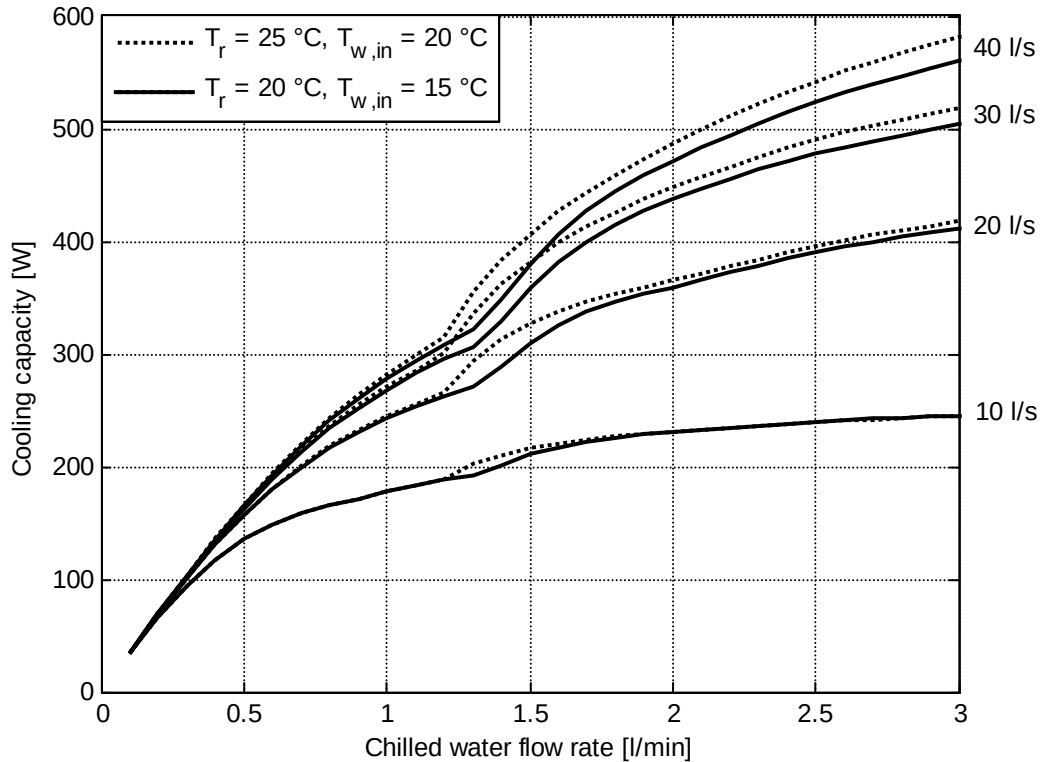
358

359 Smaller errors in the nonturbulent cases may seem strange. This is caused by the fact that all nonturbulent

360 cases were measured at the same primary airflow, level of internal heat gain and chilled water inlet

361 temperature.

362 Figure 8 presents simulated cooling capacity as a function of the chilled water flow rate at four different
 363 primary air flows and two different temperature levels. This shows how the cooling capacity is affected
 364 by the transition between laminar and turbulent flow as well as by the fact that the induction ratio is
 365 higher at higher chilled water inlet temperature.



366

367 *Figure 8 Simulated cooling capacity as a function of the chilled water flow rate at four different primary air flows and at two*
 368 *different temperature levels.*

369

370 4.5 Uncertainty analysis

371 The maximum and average uncertainties of the measured cooling capacity are estimated to be 4.1% and
 372 2.6% respectively. This includes random uncertainties (estimated from statistical analysis of the
 373 measured data) as well as systematic uncertainties (estimated from specifications declared by producers
 374 of the instruments). However, since the systematic uncertainties likely occur in a similar manner in the
 375 cases used for model calibration as in the cases used for model validation, they do not manifest
 376 themselves as inaccuracies of the model. The systematic uncertainties are approximately twice as large
 377 as the random uncertainties. This explains the fact that the estimated uncertainties of the measurements
 378 are larger than the average error of the model.

379 **5 Discussion**

380 When calibrating the model from the results of measurements, there is a trade-off between the number
381 of cases used for calibration and the accuracy of the model. The trade-off used in this study was six cases
382 including: 1) low and high chilled water temperature in order to capture how the water temperature
383 influences the IR and 2) low, medium and high primary air flow rates in order to capture how primary
384 air flow influences air-side convective heat transfer as well as the IR. Using all 48 cases for calibration
385 of the model decreases the average error from 1.7% only to 1.6%. Using only two cases (high and low
386 primary air flow rate) for calibration and assuming a constant IR on the other hand, increases the average
387 error to 2.7%. Such small error with only two cases for calibration is remarkable and indicate that the
388 major strength of the model is not the accurate determination of the IR, even though it adds extra
389 accuracy.

390 When calibrating the model, measured cooling capacity and induction ratio is required. Additionally, the
391 model need information about inner diameter and length of the coil tubes. These data are normally easily
392 obtainable.

393 Taking radiation into account when determining the IR (Equation 19) but not when calculating the overall
394 heat transfer coefficient (Equation 11) may seem inconsistent. However, the heat transferred by radiation
395 influences the unknown parameters of Equation 16 and the model simplifies the reality by making the
396 radiation proportional to a temperature difference rather than to the difference between the temperatures
397 to the fourth power. At temperature differences as small as in this application, the error from this is
398 negligible and this simplification is often applied in HVAC analysis.

399 The model shows very good correspondence with measured data in a wide range of operational
400 conditions. The ranges of operational conditions studied were chilled water supply temperature between
401 16 °C and 22 °C, room air temperature between 21 °C and 29 °C, primary air flow between 15 l/s and 35
402 l/s and chilled water flow rate between 0.4 l/min and 2.9 l/min.

403 The model is easy to implement in building performance simulation software and in contrast to most
404 ACB models, it also generates information about the temperature and flow of supply air. This information
405 is vital when simulating thermal comfort. Furthermore, supply air flow determines the convective heat
406 transfer coefficient of internal surfaces in the room [20], which Dominguez-Muñoz et al. [21] identified
407 as a major source of uncertainty when determining the peak cooling load of a building. Use of this model

408 also enables the possibility to accurately determine the actual flow of chilled water and consequently the
409 required pump power in systems where the chilled water flow rate is modulated according to the cooling
410 load. Using ACBs in combination with variable air volume systems has received increased attention
411 lately [22], [23]. The model presented in this paper is very valuable in these systems since the unknown
412 parameters are independent of operating conditions. This implies that no interpolation between operating
413 points (used for calibration) is required and the inaccuracy associated with interpolation is consequently
414 diminished.

415 This study proved the accuracy of the suggested model in cooling mode for one specific ACB operating
416 under static conditions. Further work is required in order to investigate the operation in heating mode,
417 for other types of ACBs and under dynamic conditions. The measurements were carried out in a 3.0 m
418 by 4.2 m mock-up of an office room but the results are assumed to be valid in rooms of other sizes as
419 well.

420 **Acknowledgement**

421 This paper is a result of the research project *Self-Regulating Active Chilled Beam Systems*. The project is
422 funded by the Construction Industry Organisation for Research and Development (SBUF) in Sweden.

- 424 [1] IEA (2011) Technology Roadmap. Energy-efficient Buildings. Heating and Cooling
425 Equipment. Paris, France.
- 426 [2] IEA (2012). Energy Technology Perspectives 2012, International Energy Agency. Paris, France.
427 ISBN: 978-92-64-17488-7.
- 428 [3] IEA (2016). Energy Efficiency Market Report 2016, International Energy Agency. Paris,
429 France.
- 430 [4] Santamouris, M., Papanikolaou, N., Livada, I., Koronakis, I., Georgakis, C., Argiriou, A., &
431 Assimakopoulos, D. (2001). On the impact of urban climate on the energy consumption of
432 buildings. *Solar energy*, 70(3), 201-216.
- 433 [5] Aebischer, B., Catenazzi, G., & Jakob, M. (2007). *Impact of climate change on thermal comfort,*
434 *heating and cooling energy demand in Europe*. Paper presented at the Proceedings eceee.
- 435 [6] Davis, L. W., & Gertler, P. J. (2015). Contribution of air conditioning adoption to future energy
436 use under global warming. *Proceedings of the National Academy of Sciences*, 112(19), 5962-
437 5967.
- 438 [7] Gräslund, J. (2015). Kompressorfri kyla i energieffektivt kontor. *Energi & Miljö*, 86(11), 48-
439 51.
- 440 [8] EN 15116: (2005). Ventilation in buildings - Chilled beams - Testing and rating of active chilled
441 beams, European Committee for Standardization, Brussels.
- 442 [9] EQUA Simulation AB (2013). IDA Indoor Climate and Energy 4.5 User Manual. Available at
443 <http://www.equaonline.com/iceuser/pdf/ICE45eng.pdf>.
- 444 [10] Betz, F., McNeill, J., Talbert, B., Thimmanna, H., & Repka, N. (2012). *Issues arising from the*
445 *use of chilled beams in energy models*. Paper presented at the Proceedings of 5th National
446 Conference of IBPSA-USA.
- 447 [11] Chen, C., Cai, W., Giridharan, K., & Wang, Y. (2014). A hybrid dynamic modeling of active
448 chilled beam terminal unit. *Applied Energy*, 128, 133-143.
- 449 [12] Livchak, A., & Lowell, C. (2012). Don't turn active beams into expensive diffusers. *ASHRAE*
450 *journal*, 54(4), 52-60.
- 451 [13] Maccarini, A., Hultmark, G., Vorre, A., Afshari, A., & Bergsøe, N. C. (2015). Modeling of
452 active beam units with Modelica. *Building simulation*, 1-8.
- 453 [14] De Clercq B., D. B., Van Overloop J. (2013). *Measuring and modelling heat exchange capacity*
454 *of active chilled beams*. Paper presented at the Clima 2013. 11th REHVA World Congress and
455 8th International Conference on Indoor Air Quality, Ventilation and Energy Conservation in
456 Buildings.
- 457 [15] Filipsson, P., Trüschel, A., Gräslund, J., & Dalenbäck, J. O. (2016). Induction ratio of active
458 chilled beams– Measurement methods and influencing parameters. *Energy and Buildings*, 129,
459 445-451.
- 460 [16] Kays, W. M., & London, A. L. (1984). *Compact heat exchangers*.
- 461 [17] Laskowski, R. M. (2011). The concept of a new approximate relation for heat transfer
462 effectiveness for a cross-flow heat exchanger with unmixed fluids. *Journal of Power*
463 *Technologies*, 91(2), 93.
- 464 [18] Incropera, D. (2007). Bergman, and Lavine. *Fundamentals of heat and mass transfer*.
- 465 [19] Rabehl, R. J., Mitchell, J. W., & Beckman, W. A. (1999). Parameter estimation and the use of
466 catalog data in modeling heat exchangers and coils. *HVAC&R Research*, 5(1), 3-17.
- 467 [20] Peeters, L., Beausoleil-Morrison, I., & Novoselac, A. (2011). Internal convective heat transfer
468 modeling: Critical review and discussion of experimentally derived correlations. *Energy and*
469 *Buildings*, 43(9), 2227-2239. doi: <http://dx.doi.org/10.1016/j.enbuild.2011.05.002>
- 470 [21] Domínguez-Muñoz, F., Cejudo-López, J. M., & Carrillo-Andrés, A. (2010). Uncertainty in peak
471 cooling load calculations. *Energy and Buildings*, 42(7), 1010-1018. doi:
472 <http://dx.doi.org/10.1016/j.enbuild.2010.01.013>
- 473 [22] Kim, C., Lee, J., Lee, D., & Choi, S. (2016). Optimized operation method for an active chilled
474 beam with VAV system. *Science and Technology for the Built Environment*, 22(4), 372-378.
475 doi: 10.1080/23744731.2016.1158044
- 476 [23] Chen, C., Cai, W., Wang, Y., Lin, C., & Wang, L. (2015). Operating characteristics and
477 efficiencies of an active chilled beam terminal unit under variable air volume mode. *Applied*
478 *Thermal Engineering*, 85, 71-79. doi: 10.1016/j.applthermaleng.2015.03.016